FRACTALS IN ELASTIC-PLASTIC TRANSITIONS OF RANDOM HETEROGENEOUS MATERIALS

BY

JUN LI

THESIS

Submitted in partial fulfillment of the requirements
for the degree of Master of Science in Theoretical and Applied Mechanics
in the Graduate College of the
University of Illinois at Urbana-Champaign, 2009

Urbana, Illinois

Advisor:

Professor Martin Ostoja-Starzewski

ABSTRACT

In this thesis we propose a fractal analysis methodology to study elastic-plastic transitions in random heterogeneous materials. While it is well known that many materials display fractal characteristics, very little work was done on fractals in elasto-plasticity, and so this study is one of the first attempts in that direction. Fractal patterns have been found to form in 2D aggregates of grains of either elastic-perfectly plastic type, or elastic-hardening-plastic type, or thermo-elastic-plastic class (or elastic-plastic type with residual strains). The grains are either isotropic or anisotropic, with random, spatially non-fractal perturbations in properties such as elastic/plastic moduli, yield stresses or thermal expansion coefficients (or residual strains). The flow rule of each grain follows associated plasticity with increasing loads applied through either one of three macroscopically uniform boundary conditions admitted by the Hill-Mandel condition. Following an evolution of a set of grains that have become plastic, we find that it is an evolving fractal with its fractal dimension increasing from 0 towards 2. In essence, any non-zero noise in grains' properties gives rise to fractal patterns of plastic grains. While the grains possess sharp elastic-plastic stress-strain curves, the overall stress-strain responses are curved and asymptote toward perfectly-plastic flows; all these responses display smooth transitions but, as the randomness in properties decreases to zero, they turn into conventional curves with sharp kinks of homogeneous materials. The influence of plastic hardening and thermal effects on elastic-plastic transitions are further investigated by varying model configurations. It turns out that the fractal dimension provides an optimal parameter for describing the transition patterns in a unified way for a range of different materials.

To mom and dad

ACKNOWLEDGEMENTS

I would like to express my sincerest gratitude to my advisor, Prof. Martin Ostoja-Starzewski, for all his inspiring guidance, encouragement and support throughout my graduate study. I have learnt very much from working with him and from his professionalism.

I am thankful to my colleagues, Shivakumar Iyer Ranganathan, Ying Chen, Marcus Slavenas and Hady Joumaa for their friendly assistance, interesting and helpful discussions. I also appreciate the support staff in the MechSE department, especially Kathy Smith, Laura Herriott and James Guelfi who assisted me in non-technical matters.

Finally, I express my endless gratitude to my parents, Shouguang Li and Muxian Jiang, who consistently give me love, support and motivation.

TABLE OF CONTENTS

LIST OF TABLES

LIST OF FIGURES

CHAPTER 1

INTRODUCTION

1.1 Motivation

In traditional plasticity theory metals are treated as homogeneous materials and the plastic deformation occurs whenever the stress reaches a critical (yield) level. This deterministic model is widely employed in engineering applications for its simplicity and accuracy. It implies an immediate elastic-plastic transition, characterized by a kink in the stress-strain curve, which is not physically plausible in real materials. On the other hand, with the advent of MEMS/nanotechnology that operate well below the macroscale length scales, random fluctuation effects appear and materials can not be modeled as homogeneous any more. For micro-nano devices an important task is to guarantee their working reliability, i.e., to avoid high mechanical/thermal stresses that may induce large plastic deformation or even fracture and damage. All of these observations motivate our study of elastic-plastic transitions in random heterogeneous materials. When material randomness is taken into account, the elastic-plastic transition becomes a gradual process and its pattern may be rather complex – these are clearly due to material inhomogeneities that act as either obstacles or facilitators for the transition taking place and the elastoplastic response is essentially nonlinear. In this thesis we propose a fractal analysis methodology to study the elastic-plastic transition patterns.

It is well known that many materials display fractal characteristics (e.g., [1,2]). Indeed, fractals have been used in the characterization as well as morphogenesis models of spatial patterns. Numerous such phenomena, both in natural and artificial materials, include phase transitions and accretion [3], fracture surfaces [4-7], and dislocation patterns [8]. Of course, this is but a short list

of such studies, which were extensively conducted in the eighties and nineties. While very little work was done on fractals in elasto-plasticity, except for plastic ridges in ice fields [9] and shear bands in rocks of Mohr-Coulomb type [10,11]. Thus, the present study is a first attempt of applying fractals in elastic-plastic transitions.

When fractal concepts are employed in applications, two questions should be addressed: (i) Is the object really a fractal? (ii) Can we obtain any new physical insights from the fractal view point? A compelling feature of any fractal is its fractal dimension, a parameter which is generally not an integer and indicating the extent of its space-filling (or plane-filling) tendency. Given the complexity of mathematical techniques for analysis of elastic-plastic transitions, we numerically determine the transition process and estimate fractal dimensions of evolving sets of plastic regions. The fractal dimension is then directly related to the development of the transition both in terms of the response curve and spatial plastic patterns.

1.2 Thesis outline

In the subsequent chapters, we conduct the study in different random materials following this sequence:

(a) In Chapter 2 we consider elastic-plastic transitions in random linear elastic-perfectly plastic media. Plastic regions are found to form fractal patterns in two models studied – isotropic grains and anisotropic polycrystals. The robustness of this result among several related cases is further demonstrated.

(b) Chapter 3 discusses the plastic hardening effects in elastic-plastic transitions. The focus is on isotropic grains and various cases where different material configurations are compared to illustrate the results.

(c) Chapter 4 extends the study to thermo elastic-plastic media (or elastic-plastic type with residual strains). The transition patterns under different model randomness and material

constants are investigated by virtue of fractal dimension parameters.

(d) In Chapter 5 the main conclusions are summarized and future research directions are discussed.

CHAPTER 2

FRACTAL PATTERN FORMATION IN ELASTIC-PERFECTLY PLASTIC MATERIALS

In this chapter, we report on fractal patterns of plastic grains forming at elastic-plastic transitions in random elastic-perfectly plastic materials. Specifically, two models are considered: (1) a composite made of locally isotropic grains with weak random fluctuations in elastic moduli and/or yield limits and (2) a polycrystal made of randomly oriented anisotropic grains. The spatial assignment of material randomness follows a non-fractal strict-white-noise field on a 256×256 lattice aggregate of homogeneous square-shaped grains. These lattices are subjected to pure shear loading increasing through either one of three macroscopically uniform boundary conditions (kinematic, mixed-orthogonal or static) admitted by the Hill-Mandel condition. Following the evolution of a set of plastic grains, we find that it has a fractal dimension increasing from 0 towards 2 as the material transitions from elastic to plastic. While the grains possess sharp elastic-plastic stress-strain curves, the overall responses are smooth and asymptote toward perfectly-plastic flows; these responses and the fractal dimension-strain curves are almost identical for three different loadings[1].

2.1 Introduction

The present study focuses on elastic-plastic transitions in planar random materials made of linear elastic/perfectly-plastic phases of metal type. As a first step towards fractals in elastoplastic materials, we resort to the simplest case of perfectly plastic media. Two special types of

---

[1] See also, [12] Li, J. and Ostoja-Starzewski, M., 2010. Fractal pattern formation at elastic-plastic transition in heterogeneous materials, *ASME J. Appl. Mech.* **77**, 021005-1-7.

microstructural models are employed in our study: (1) a linear elastic-perfectly plastic material with isotropic grains having random yield limits and/or elastic moduli and (2) a ploycrystal with anisotropic grains following Hill's yield criterion and having random orientations. In both cases, the microstructures are non-fractal random fields, the reason for that assumption being that the evolution of plastic zones would obviously (or very likely) be fractal should the material properties be fractally distributed at the outset. We pose three questions: (a) Does the elastic-plastic transition occur as a fractal, plane-filling process of plastic zones with increasing macroscopically uniform applied loading? (b) What are the differences between a composite made of locally isotropic grains and a polycrystalline-type aggregate made of anisotropic grains? (c) To what extent is the fractal character of plastic zones robust under changes of the model such as the change of perturbations in material properties?

To answer these questions, we set up three types of monotonic loadings consistent with the Hill-Mandel condition, which guarantees the equivalence between energetically and mechanically defined effective responses in random heterogeneous materials [13,14]. The stress-strain responses are then numerically obtained and directly related to fractal dimensions of evolving sets of plastic grains. In all the cases we study, it turns out that the elastic-plastic transition occurs through a fractal set of plastic grains, gradually plane-filling the entire material domain. In the first model with isotropic grains, we further investigate several related cases by varying material randomness.

2.2 Model formulation

2.2.1 Random material

By a random heterogeneous material we understand a set $\mathbf{B} = \{B(\omega); \omega \in \Omega\}$ of deterministic media $B(\omega)$, where ω indicates a realization and Ω is an underlying sample space [15]. The material parameters of any microstructure, such as the elasticity tensor or the yield tensor, jointly

form a random field Θ which is required to be mean-ergodic on (very) large scales, that is

$$\overline{\mathbf{G}(\omega)} \equiv \lim_{L \to \infty} \frac{1}{V} \int_V \mathbf{G}(\omega, \mathbf{x}) dV = \int_\Omega \mathbf{G}(\omega, \mathbf{x}) dP(\omega) \equiv \langle \mathbf{G}(\mathbf{x}) \rangle \tag{2.1}$$

Here and after the overbar indicates the volume average and $\langle \ \rangle$ means the ensemble average. $P(\omega)$ is the probability measure assigned to the ensemble $\{G(\omega, \mathbf{x}); \omega \in \Omega, \mathbf{x} \in V\}$ and its σ–algebra.

The microstructures in our study are linear elastic/perfectly-plastic materials with an associated flow rule. Specifically, the constitutive response of any grain [i.e. a piecewise-constant region in a deterministic microstructure $B(\omega)$] is described by

$$d\boldsymbol{\varepsilon} = \mathbf{D}^{-1} d\boldsymbol{\sigma} + \dot{\lambda} \frac{\partial f_p}{\partial \boldsymbol{\sigma}} \quad \text{when} \ \ f_p = 0 \ \ \text{and} \ \ df_p = 0,$$
$$d\boldsymbol{\varepsilon} = \mathbf{D}^{-1} d\boldsymbol{\sigma} \quad \text{when} \ \ f_p < 0, \ \ \text{or} \ \ f_p = 0 \ \ \text{and} \ \ df_p < 0. \tag{2.2}$$

where $\mathbf{D}$ is the elasticity tensor and f_p is the yield function. For anisotropic materials with quadratic yielding, f_p is taken in the form

$$f_p = \Pi_{ijkl} \sigma_{ij} \sigma_{kl} - 1. \tag{2.3}$$

Here Π_{ijkl} represents a positive defined fourth-order yield tensor with the following symmetries

$$\Pi_{ijkl} = \Pi_{jikl} = \Pi_{ijlk} = \Pi_{klij} \tag{2.4}$$

It follows that Π_{ijkl} has only 21 independent components instead of 81 components in the most general case. The following two special forms of Eq. (2.3) will be employed:

(i) Huber-von Mises-Hencky (isotropic) yield criterion

$$f_p = \frac{1}{6} \left[(\sigma_{11} - \sigma_{22})^2 + (\sigma_{11} - \sigma_{33})^2 + (\sigma_{22} - \sigma_{33})^2 \right] + \sigma_{12}^2 + \sigma_{13}^2 + \sigma_{23}^2 - \frac{\sigma_0^2}{3} \tag{2.5}$$

(ii) Hill (orthotropic) yield criterion

$$f_p = F(\sigma_{11} - \sigma_{22})^2 + G(\sigma_{11} - \sigma_{33})^2 + H(\sigma_{22} - \sigma_{33})^2 + 2L\sigma_{12}^2 + 2M\sigma_{13}^2 + 2N\sigma_{23}^2 - 1 \tag{2.6}$$

2.2.2 Hill condition

Key issues in the mechanics of random materials revolve around effective responses, scales on

which they are attained, and types of loading involved. The Hill condition establishes the equivalence (compatibility) of energetically and mechanically defined effective responses in linear elastic heterogeneous materials [13] i.e., $\overline{\boldsymbol{\sigma}:\boldsymbol{\varepsilon}} = \overline{\boldsymbol{\sigma}}:\overline{\boldsymbol{\varepsilon}}$. It can be generalized to elastic-plastic materials in an incremental setting [14,15]. To understand this, we consider a nonlinear inelastic material, where the strain energy can be specified by a functional F

$$F = \boldsymbol{\sigma} * \boldsymbol{\varepsilon} \tag{2.7}$$

Here * is a linear operator depending on particular cases. The constitutive relations are expressed as

$$\boldsymbol{\sigma} = \boldsymbol{\varphi}(\boldsymbol{\varepsilon}), \quad \boldsymbol{\varepsilon} = \boldsymbol{\psi}(\boldsymbol{\sigma}) \tag{2.8}$$

Now we introduce the energetic and mechanical effective properties, denoted by e and m in superscripts, respectively

$$\overline{F} = \boldsymbol{\varphi}^{e}\left(\overline{\boldsymbol{\varepsilon}}\right) * \overline{\boldsymbol{\varepsilon}} \tag{2.9}$$

$$\overline{\boldsymbol{\sigma}} = \boldsymbol{\varphi}^{m}\left(\overline{\boldsymbol{\varepsilon}}\right), \quad \overline{\boldsymbol{\varepsilon}} = \boldsymbol{\psi}^{m}\left(\overline{\boldsymbol{\sigma}}\right) \tag{2.10}$$

Substituting (2.10) into (2.9) we obtain

$$\overline{F} = \boldsymbol{\varphi}^{e}\left(\overline{\boldsymbol{\varepsilon}}\right) * \overline{\boldsymbol{\varepsilon}} = \boldsymbol{\varphi}^{e}\left(\boldsymbol{\psi}^{m}\left(\overline{\boldsymbol{\sigma}}\right)\right) * \overline{\boldsymbol{\varepsilon}} \tag{2.11}$$

Note that the equivalence of energetic and mechanical effective properties requires $\boldsymbol{\varphi}^{e} = \boldsymbol{\varphi}^{m}$. In addition to $\boldsymbol{\psi}^{m} = \left(\boldsymbol{\varphi}^{m}\right)^{-1}$, it yields

$$\overline{F} = \overline{\boldsymbol{\sigma}} * \overline{\boldsymbol{\varepsilon}} \quad \text{i.e.,} \quad \overline{\boldsymbol{\sigma} * \boldsymbol{\varepsilon}} = \overline{\boldsymbol{\sigma}} * \overline{\boldsymbol{\varepsilon}} \tag{2.12}$$

Equation (2.12) is the generalized form of Hill condition in nonlinear and inelastic materials. For elastic-plastic materials it takes the form

$$\overline{\int \boldsymbol{\sigma} : d\boldsymbol{\varepsilon}} = \int \overline{\boldsymbol{\sigma}} : d\overline{\boldsymbol{\varepsilon}} \tag{2.13}$$

Transforming the volume integral to integrals over the boundary by the Gauss theorem, we obtain

$$\int_{\partial B_{\delta}} \left(\mathbf{t} - \overline{\boldsymbol{\sigma}} \cdot \mathbf{n}\right) \cdot \left(d\mathbf{u} - d\overline{\boldsymbol{\varepsilon}} \cdot \mathbf{x}\right) dS = 0 \tag{2.14}$$

where $\mathbf{u}$ is the displacement vector and $\mathbf{t}$ is the traction vector on the specimen boundary ∂B_{δ}. Equation (2.14) suggests three special types of uniform boundary conditions (BCs):

(1) kinematic (displacement) BC (with applied constant incremental strain $d\bar{\boldsymbol{\varepsilon}}$):

$$d\mathbf{u} = d\bar{\boldsymbol{\varepsilon}} \cdot \mathbf{x}, \qquad \forall \mathbf{x} \in \partial B_{\delta}; \tag{2.15}$$

(2) static (traction) BC (with applied constant stress $\bar{\boldsymbol{\sigma}}$):

$$\mathbf{t} = \bar{\boldsymbol{\sigma}} \cdot \mathbf{n}, \qquad \forall \mathbf{x} \in \partial B_{\delta}; \tag{2.16}$$

(3) mixed-orthogonal (or displacement-traction) BC:

$$(\mathbf{t} - \bar{\boldsymbol{\sigma}} \cdot \mathbf{n}) \cdot (d\mathbf{u} - d\bar{\boldsymbol{\varepsilon}} \cdot \mathbf{x}) = 0, \forall \mathbf{x} \in \partial B_{\delta}. \tag{2.17}$$

Note here that an unambiguous way of writing (2.17) involves orthogonal projections [16]

$$\left(\mathbf{u} - \mathbf{u}^{0}\right) \cdot \mathbf{n} = 0, \quad \left(\mathbf{I} - \mathbf{n} \otimes \mathbf{n}\right)\left(\boldsymbol{\sigma}(\mathbf{u}) \cdot \mathbf{n} - \mathbf{t}^{0}\right) = 0. \tag{2.18}$$

In this case, the formal boundary vector is of mixed structure, i.e., it has one or two components imposed by boundary displacements and the lacking components by tractions. Strictly speaking, the static BC (2.16) is ill-posed for a perfectly-plastic material, but all the materials in our study are heterogeneous, so that the overall stress-strain responses will effectively be the hardening-type for monotonic loadings. We return to this issue in Sec. 2.3.

2.2.3 Hierarchy of mesoscale bounds

When the size of a specimen is smaller than the RVE, the volume averaged responses must be referred as apparent, rather than effective [17]. Some fundamental questions will be posed, "How close are the apparent properties related to the effective properties?", and "How big is the size of a specimen enough to approximately attain an RVE?" One possible way is to set up different boundary value problems which are consistent with the Hill condition and bound the effective responses from above and below. When the bounds become very tight (almost identical) we say that the RVE is approximately obtained. A hierarchy of bounds on the effective tangent stiffness tensor $\mathbf{C}^{Teff}$ shows

$$\begin{aligned} &\left\langle \mathbf{S}_{1}^{Tt} \right\rangle^{-1} \le \dots \le \left\langle \mathbf{S}_{\delta'}^{Tt} \right\rangle^{-1} \le \left\langle \mathbf{S}_{\delta}^{Tt} \right\rangle^{-1} \le \dots \le \left(\mathbf{S}_{\infty}^{Tt}\right)^{-1} \equiv \mathbf{C}^{Teff} \\ &\equiv \mathbf{C}_{\infty}^{Td} \le \dots \le \left\langle \mathbf{C}_{\delta}^{Td} \right\rangle \le \left\langle \mathbf{C}_{\delta'}^{Td} \right\rangle \le \dots \le \left\langle \mathbf{C}_{1}^{Td} \right\rangle, \quad \text{for all} \quad 1 \le \sigma' < \sigma \le \infty. \end{aligned} \tag{2.19}$$

Here $\left\langle \mathbf{C}_\delta^{Td} \right\rangle$ and $\left\langle \mathbf{S}_\delta^{Tt} \right\rangle$ are the apparent tangent stiffness and compliance moduli, respectively. The superscript d (or t) indicates the case of displacement (or traction) BC. Another type of hierarchy that applies is in terms of energies (see Eq. (15) in [18]). Hazanov and Huet [19] exemplified the case of mixed-orthogonal BCs, in which the apparent moduli are bounded from above and below by those under displacement and traction BCs. A proof of inequalities (2.19) for elastoplastic materials is shown in [20]. Here we simply sketch the proof in linear elastic materials as follows.

Consider a partition of a square-shaped window $B_\delta(\omega)$ of volume V_δ into four smaller parts $B_{\delta'}^s(\omega)$, $s = 1,\dots,4$ of size $\delta' = \delta/2$ and volume $V_{\delta'}$ each. Note that the boundary conditions of the latter are more restricted than the original case since they are applied to the boundaries of all $B_{\delta'}^s(\omega)$ rather than $B_\delta(\omega)$. Now, following the minimum energy principles we have:

$$w\left(\overline{\mathbf{\varepsilon}}, \delta\right) \le w\left(\overline{\mathbf{\varepsilon}}, \delta'\right) \tag{2.20}$$

For linear elastic materials, it shows that

$$\frac{1}{2} V_\delta \overline{\mathbf{\varepsilon}} : \mathbf{C}_\delta^d : \overline{\mathbf{\varepsilon}} \le \sum_{s=1}^4 \frac{1}{2} V_{\delta'} \overline{\mathbf{\varepsilon}} : \mathbf{C}_{\delta'}^{d,s} : \overline{\mathbf{\varepsilon}} \tag{2.21}$$

Here $\mathbf{C}_\delta^d$ and $\mathbf{C}_{\delta'}^{d,s}$ are the apparent stiffness tensors of $B_\delta(\omega)$ and $B_{\delta'}^s(\omega)$, respectively. Upon volume averaging we obtain

$$\left\langle \mathbf{C}_\delta^d \right\rangle \le \left\langle \mathbf{C}_{\delta'}^d \right\rangle \tag{2.22}$$

In this way, a sequence of upper δ-dependent bounds is obtained on $\mathbf{C}^{eff} \equiv \mathbf{C}_\infty^d$. Similarly, applying to the complementary energy in traction BCs, we have

$$\left\langle S_\delta^t \right\rangle \le \left\langle S_{\delta'}^t \right\rangle \tag{2.23}$$

The sequence of lower δ-dependent bounds on $\mathbf{C}^{eff}$ is obtained by simply inverting (2.23). Therefore we obtain the hierarchy (2.19).

2.3 Computational simulations of elastic-plastic transitions

We consider two special models of such random heterogeneous materials. One consists of isotropic grains and the other is an aggregate of anisotropic grains (crystals). In both cases, the grains are homogeneous, linear elastic/perfectly-plastic with the flow rule following associated plasticity. The Huber-von Mises-Hencky yield criterion applies to isotropic grains, while for crystals we employ Hill's quadratic orthotropic yielding.

Model 1 (isotropic material): Isotropic grains with random perturbations in the elastic modulus and/or the yield limit. It follows that the random field of material properties is simplified to $\Theta = \{E, \sigma_0\}$, in which E is the elastic modulus and σ_0 represents the yield stress. The spatial assignment of random E and/or σ_0 is a field of independent identically distributed (i.i.d.) random variables. That is, $\Theta = \{E, \sigma_0\}$ is a strict-white-noise field, clearly non-fractal. Their mean values are those of aluminum: $E = 71\,\mathrm{GPa}$, $\sigma_0 = 137\,\mathrm{MPa}$, with the Poisson ratio $\upsilon = 0.348$ [21].

Model 2 (anisotropic material): Anisotropic polycrystalline aggregates with random orientations. For individual crystals the elasticity tensor $\mathbf{D}^p$ and the yield tensor $\mathbf{\Pi}^p$ are given by

$$\begin{aligned}
\mathbf{D}_{ijkl}^{p} &= \mathbf{R}_{im}^{p}\mathbf{R}_{jn}^{p}\mathbf{R}_{kr}^{p}\mathbf{R}_{ls}^{p}\mathbf{D}_{mnrs}^{ref}, \\
\mathbf{\Pi}_{ijkl}^{p} &= \mathbf{R}_{im}^{p}\mathbf{R}_{jn}^{p}\mathbf{R}_{kr}^{p}\mathbf{R}_{ls}^{p}\mathbf{\Pi}_{mnrs}^{ref}.
\end{aligned} \tag{2.24}$$

where $\mathbf{D}^{ref}$ and $\mathbf{\Pi}^{ref}$ are the referential elasticity and yield tensor and $\mathbf{R}^p$ is the rotation tensor associated with a grain of type p. Also in this model, the random orientations form a strict-white-noise field. The material orientations are taken to be uniformly distributed on a circle; this is realized by an algorithm of Shoemake [22]. Values of the referential material parameters are given in Table 2.1.

A numerical study of both models, in plane strain, is carried out by a finite element method (FEM) commercial software ABAQUS [23]. We take a sufficiently large domain that comprises 256×256 square-shaped grains. In model 1 we keep E constant and let σ_0 be a uniform

random variable of up to $\pm2.5\%$ about the mean. Other kinds of material randomness are studied in Sec. 2.5. We apply shear loading through one of the three types of uniform BC:

$$\text{Kinematic: } \varepsilon_{11}^0 = -\varepsilon_{22}^0 = \varepsilon, \ \varepsilon_{12}^0 = 0,$$
$$\text{Mixed: } \varepsilon_{11}^0 = \varepsilon, \sigma_{22}^0 = -\sigma, \varepsilon_{12}^0 = \sigma_{12}^0 = 0, \quad (2.25)$$
$$\text{Static: } \sigma_{11}^0 = -\sigma_{22}^0 = \sigma, \ \sigma_{12}^0 = 0.$$

all consistent with Eqs. (2.15)-(2.17).

The equivalent plastic strain contour plots under different BCs are shown in Fig. 2.1 for both models on domains 64×64 grains; these smaller domains are chosen because graphics on larger domains become too fuzzy visually. We can find that the shear bands are at roughly 45^0 to the direction of tensile loading under various BCs. This is understandable since we apply shear loading with equal amplitude in both directions, while the material field is inhomogeneous, so the shear bands are not at 45^0 exactly. Regarding this inhomogeneity, the plastic grains tend to form in a geodesic fashion so as to avoid the stronger grains [24]. Note that the shear band patterns under the three BCs are different. They differ by stress concentration factors and rank in the following order in terms of BCs: kinematic, mixed and static.

Figures 2.2 (a,b) show constitutive responses of volume-averaged stress and strain under three BCs for both models. The responses of single grain homogenous phases are also given for a reference. First, the curves under different BCs almost overlap, showing that the (256×256) domain is very close to the RVE, i.e. the responses are almost independent of the type of BCs [15,25]. Of course, domains as large as possible are needed to assess fractal dimensions. The response under mixed-orthogonal loading is bounded from above and below by kinematic and static loadings, respectively. The results also verify the hierarchy of mesoscale bounds (2.19).

Note that the curves of heterogeneous materials are always bounded from above by those of the corresponding homogeneous materials. However, the difference in the case of model 2 is larger - the reason for this is that, while in model 1 we use a material whose parameters are

arithmetic means of the microstructure, in model 2 we have to use a material with all crystalline grains aligned in one direction ($\mathbf{R}^p = \mathbf{I}$).

2.4 Fractal patterns of plastic grains

Figures 2.3(a, b, c, d) show elastic-plastic transition patterns in model 2 for increasing stress σ in static BC. The figures use a binary format in the sense that elastic grains are white, while the plastic ones are black. The plastic grains form plastic regions of various shapes and sizes, and we estimate their fractal dimension D using a "box-counting method" [26]:

$$D = -\frac{\log(N_r)}{\log(r)} \tag{2.26}$$

where Nr denotes the number of boxes of size r needed to cover the object. We developed a computer code for the box-counting method and verified it in a typical example of the Sierpiński Carpet. This fractal object is obtained by dividing a square into nine subsquares, removing the central square, and repeating the same type of division on the remaining subsquares in a self-similar way across an infinite range of scales. Figure 2.4 shows an approximation of the Sierpiński Carpet obtained after six iterations on the resolution level 729×729. The fractal dimension D is log(8)/log(3)=1.8923. Our estimation gives D=1.8911, showing a good agreement.

The results of box counts for Figs. 2.3(a, b, c, d) are shown in Figs. 2.5(a, b, c, d), respectively, where we plot the *ln-ln* relationship between the box number Nr and the box size r, respectively. With the correlation coefficients very close to 1.0 for all four figures, we conclude that the elastic-plastic transition patterns are fractal. The same type of results, except for the fact that the spread of plastic grains is initially slower under the static BC, is obtained for two other loadings in model 2 as well as all loadings in model 1.

Figures 2.6(a, b) show evolutions in time of the fractal dimension D under different BCs for both material models. We find that the curves depend somewhat on a particular BC: in both

models the fractal dimension D grows slower under the static BC than under the mixed BC, and then the kinematic BC. However, note that they share a common trend regardless of the loading applied: D tends to 2.0 during the transition, showing that the plastic grains have a tendency to spread over the entire material domain.

Furthermore, the dependencies of D on the volume averaged plastic strain under different BCs are almost identical in the case of both models, Fig. 2.7. This is very similar to the materials' constitutive responses - say, the volume averaged stress *vs.* strain - which are independent of BCs for sufficiently large domains in Fig. 2.2. Thus, D turns out to be a useful parameter in quantifying the evolution of elastic-plastic transitions in heterogeneous materials at and above the RVE level.

2.5 Further discussion of model 1

Here we examine model 1 under several kinds of material parameter randomness and various model assumptions. First, the sensitivity of transition patterns to the material's model randomness is investigated through comparisons in two scenarios:

Scenario A: Scalar random field of the yield limit, with three types of randomness:

A1 - Yield limit is a uniform random variable of up to $\pm 2.5\%$ about the mean.

A2 - Yield limit is a uniform random variable of up to $\pm 0.5\%$ about the mean.

A3 - Deterministic case: no randomness in the yield limit.

Scenario B: Random field of the yield limit and/or elastic moduli $\Theta_p = \{E_p, \sigma_p\}$, with three cases:

B1 = A1.

B2 – Elastic moduli is a uniform random variable of up to $\pm 2.5\%$ about the mean.

B3 – Yield limits and elastic moduli are independent uniform random variables of up to $\pm 2.5\%$ about their means.

Results for A1-A3 and B1-B3 are shown in Figs. 2.8 and 2.9, respectively. From Figs. 2.8(a,b)

one can conclude that different random variants in the model configuration lead to different transition patterns; overall, a lower randomness results in a narrower elastic-plastic transition. Next, in Fig. 2.9 we observe the randomness in yield limits to have a stronger effect than that in elastic moduli. When both these properties are randomly perturbed, the effect is even stronger– both, in the curves of the average stress as well as the fractal dimension versus the average plastic strain.

A test of the robustness of results of model 1 involves a comparison of the original material with two other cases: (i) a hypothetical material with parameters of the aluminum increased by factor 2 ($E = 142\,\mathrm{GPa}$, $\sigma_0 = 274\,\mathrm{MPa}$) and (ii) a material with parameters of mild steel in ($E = 206\,\mathrm{GPa}$, $\sigma_0 = 167\,\mathrm{MPa}$) [21]. Figure 2.10(a) illustrates the evolutions of D with respect to plastic strain for these materials. One can find that the curves of material 1 and 2 are almost identical and bounded from above by that of material 3, which is understandable, since the first two materials have the same yield strain while for the latter one it is less than the two.

In order to demonstrate the influence of yield strain more clearly, we scale the plastic strain by material's yield strain and plot the results again in Fig. 2.10(b). The three curves are now practically identical. Note that, after scaling of yield strain, the constitutive responses of all variants of model 1 are also reduced to one smooth stress-strain curve, which can be fitted by, say, $\sigma_{12} = (2k / \pi) \tan^{-1} (d_{12} / b)$, where k is the yield stress in shear, while $b > 0$ models a smooth curve; for $b \to 0$, the smooth curve tends towards the line of perfect plasticity. This curve may be bounded by the linear elasticity/perfect plasticity with yield strain equal to 1.0.

2.6 Summary

The work performed in this chapter is the first step to study fractal patterns at elastic-plastic transitions in heterogeneous materials. We consider random linear elastic/perfectly-plastic media, where the yield limits and/or elastic moduli are taken as non-fractal, random fields (in fact, fields of i.i.d. random variables). In particular, two planar models are studied: a composite with isotropic

grains and a polycrystal with anisotropic grains having orientation-dependent elasticity and Hill's yield criterion. By setting up three types of loadings consistent with the Hill-Mandel condition, the stress-strain responses and fractal dimensions of evolving plastic regions are obtained by computational simulations. Referring to the three questions raised in the Introduction of this chapter, we find the following:

(a) The elastic-plastic transition occurs as a fractal, plane-filling process of plastic zones in both heterogeneous (fundamentally non-fractal) material models – one with random fluctuations in yield limits and/or elastic moduli, and another with randomly oriented anisotropic grains. The fractal dimension of plastic zones increases monotonically as the macroscopically applied loading increases, with kinematic BC in a strongest growth of D, followed by the mixed-orthogonal BC, and then by the static BC.

(b) Very similar fractal patterns and stress-strain curves are exhibited by both, the composite made of locally isotropic grains and the polycrystalline aggregate made of anisotropic grains. As the randomness in material properties decreases towards zero in the first model, the elastic-plastic transition tends from a smooth curved bend in the effective stress-strain curve towards a sharp kink and this is accompanied by an immediate plane-filling of plastic zones. Of course, the limiting case of no spatial randomness does not physically exist, i.e., a homogeneous material is but a hypothetical, idealized model. Also note that, in the model with anisotropic grains, no sharp kink can be recovered unless all the grains acquire an identical orientation.

(c) The fractal character of plastic zones is robust under changes of the model such as the change in strength in random perturbations in material properties or a change in the mean elastic moduli and yield limits. Since in all the cases the elastic-plastic transitions share a common trend (0 towards 2), the fractal dimension D turns out to be an optimal parameter to investigate transition patterns among different materials.

While this study is set in the context of elastic-perfectly plastic grains, the next step will have

to show, among others, how hardening affects the plane filling of plastic zones, and how fractal patterns change when thermo effects (or residual strains) are taken into account. Those topics will be discussed in the next two chapters successively.

Table 2.1: Material parameters in Model 2.

Material	Elasticity[a] (GPa)			Plasticity[b]				
	c_{11}	c_{12}	c_{44}	σ_0(MPa)	σ_{11}/σ_0	σ_{22}/σ_0	σ_{33}/σ_0	σ_{12}/σ_0
Aluminum	108	62.2	28.4	137	1.0	0.9958	0.9214	1.08585

[a] Material properties for cubic elastic symmetry [27].

[b] Material properties for the quadratic anisotropic yield criterion [21].
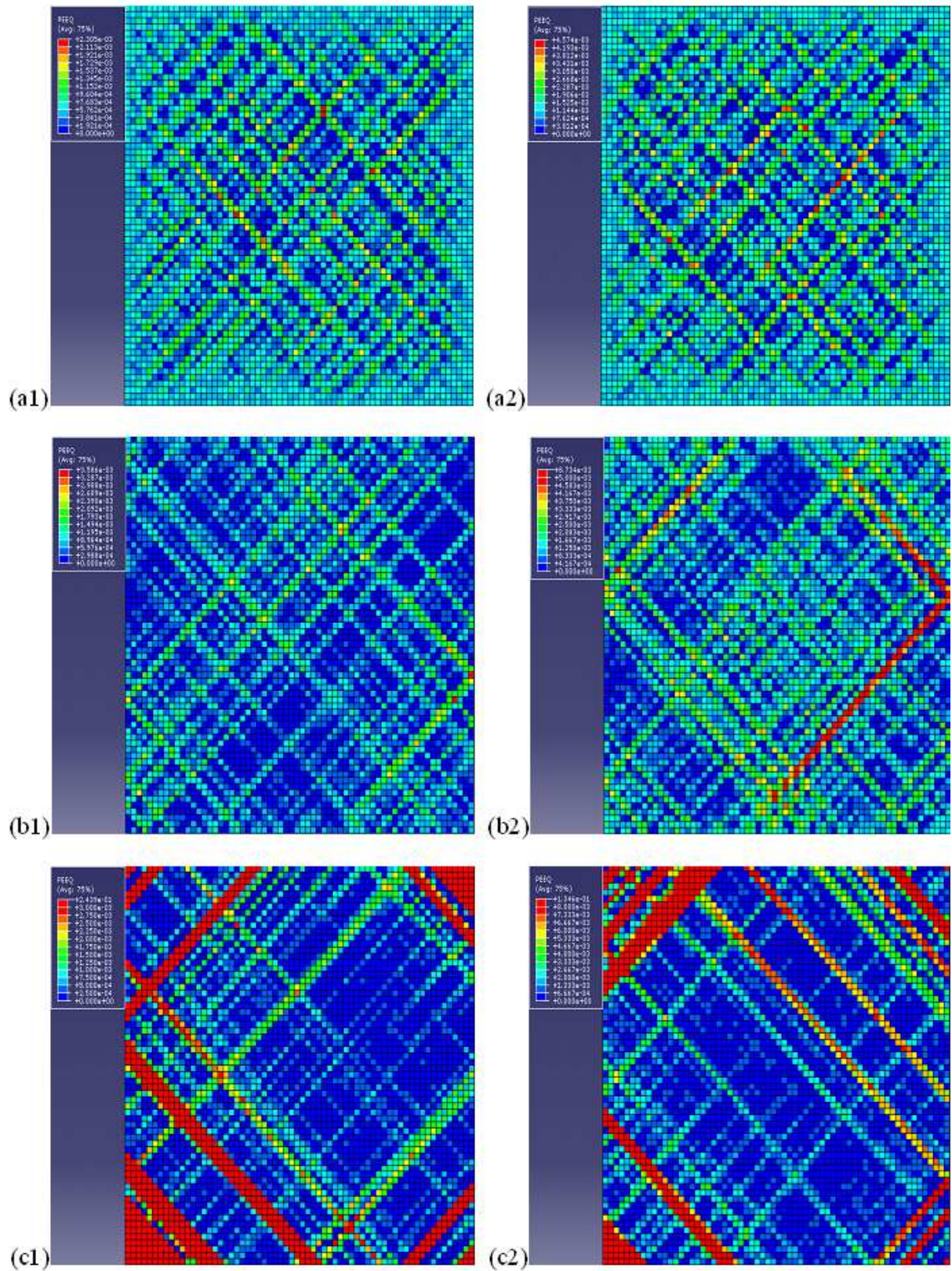
Figure 2.1: Plots of equivalent plastic strain on 64×64 domains for model 1 (isotropic grains) and model 2 (anisotropic grains) under various BCs: (a1,a2) kinematic, (b1,b2) mixed, and (c1,c2) static.
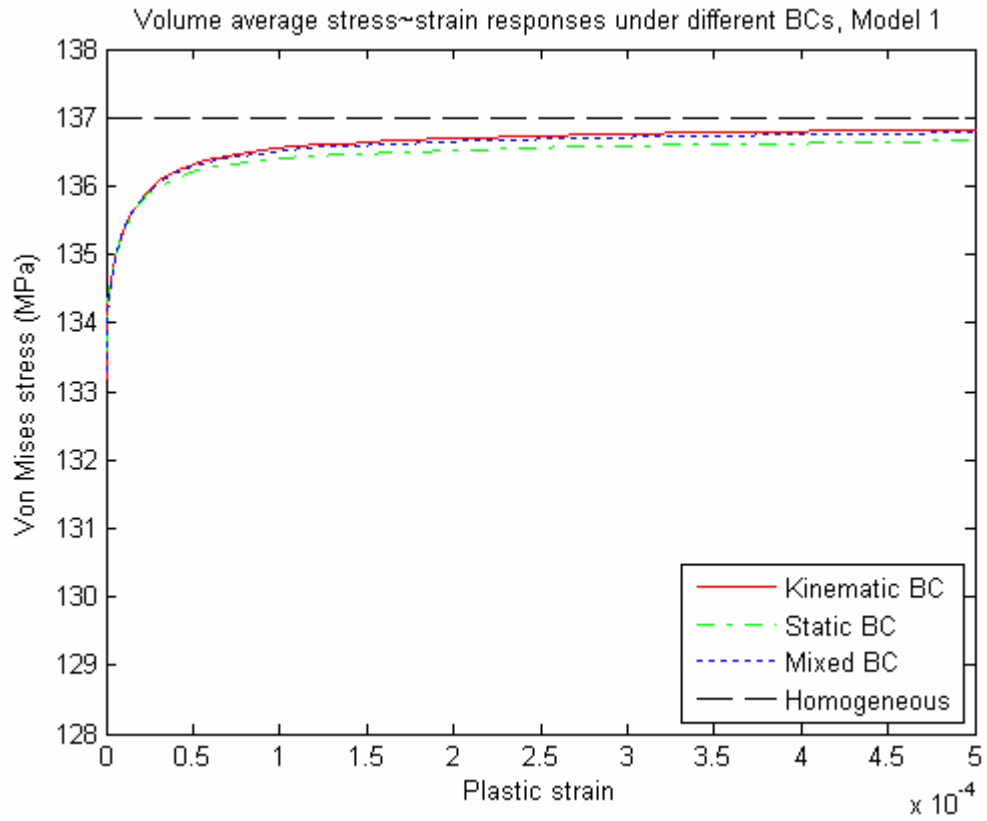
(a)
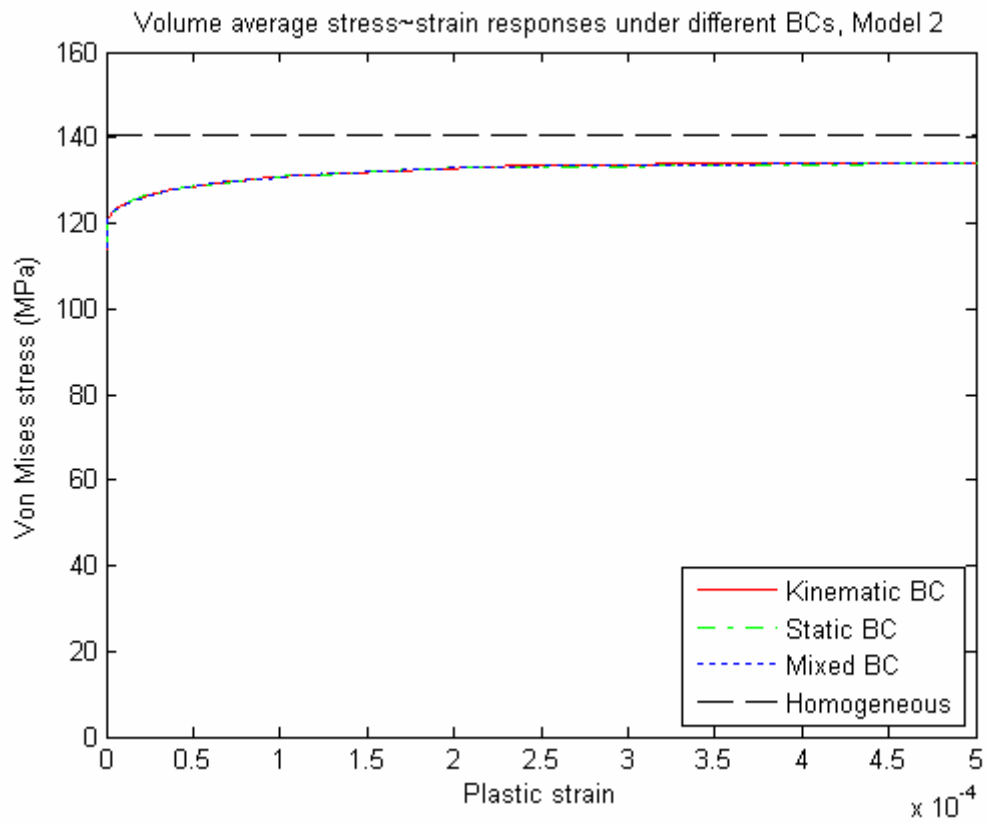
(b)

Figure 2.2: Volume-averaged stress~strain responses under different BCs for: (a) model 1 (isotropic grains) and (b) model 2 (anisotropic grains).
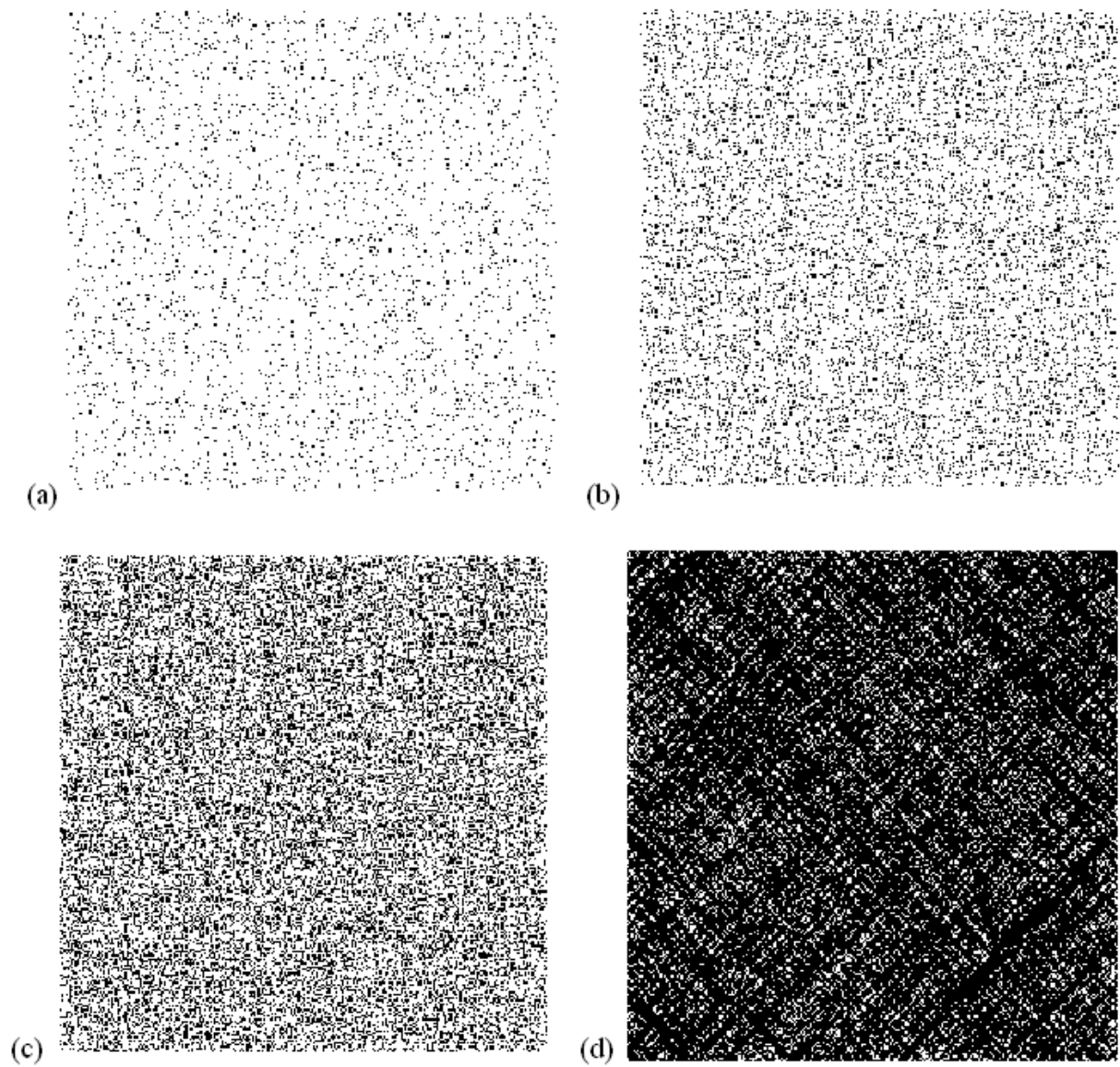
Figure 2.3: Field images (white: elastic; black: plastic) for model 2 (anisotropic grains) at four consecutive stress levels applied via uniform static BC. The set of black grains is an evolving set, with the fractal dimension given in Figs. 2.5(a-d).
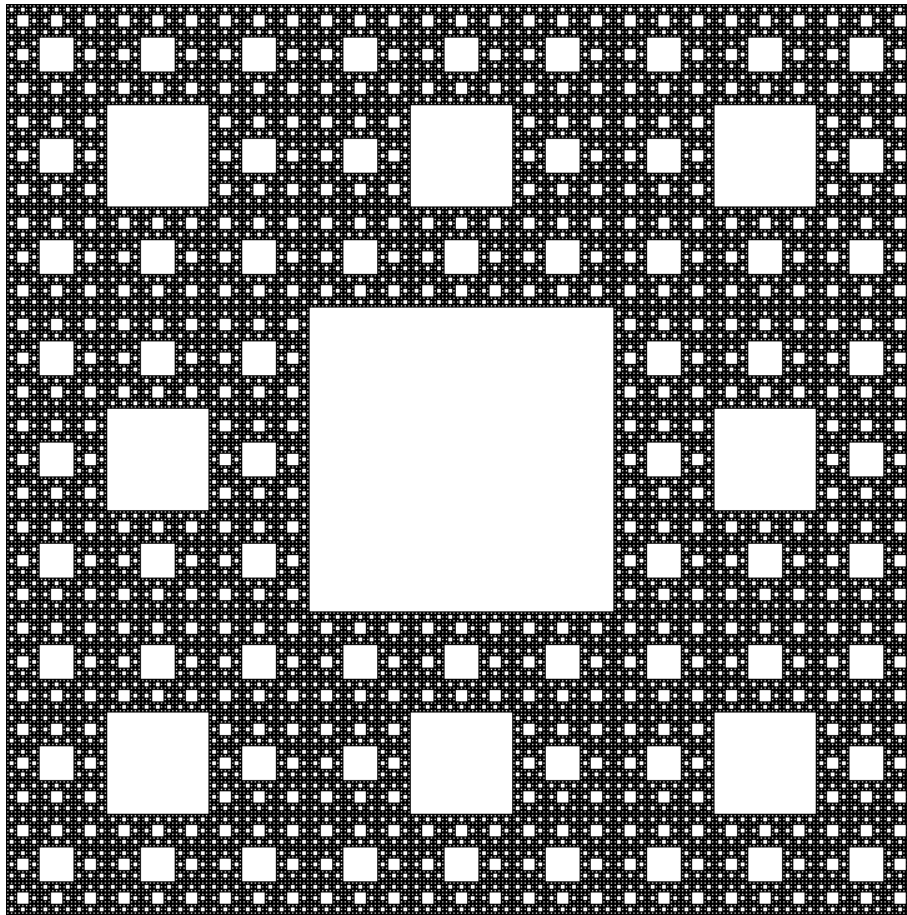
Figure 2.4: A fractal example to test our computer code: Sierpiński Carpet on 729×729 pixels.

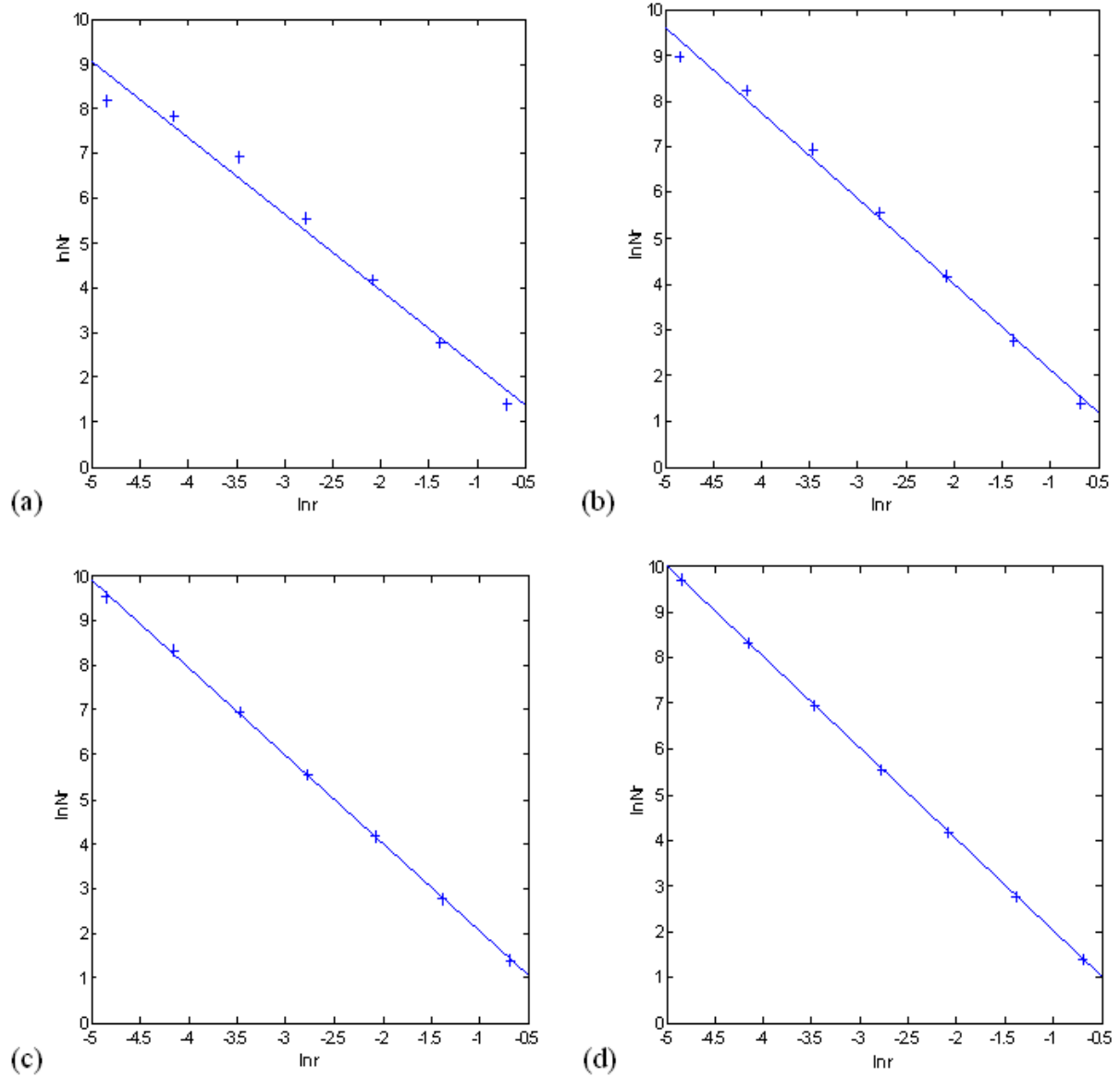The theoretical value is log(8)/log(3)=1.8923 and our estimation gives D=1.8911.

Figure 2.5: Estimation of the fractal dimension *D* for Figs. 2.3(a-d), respectively, using the box-counting method: (a) $D = 1.667$, (b) $D = 1.901$, (c) $D = 1.975$, (d) $D = 1.999$. The lines correspond to the best linear fitting of *ln(Nr)* versus *ln(r)*.
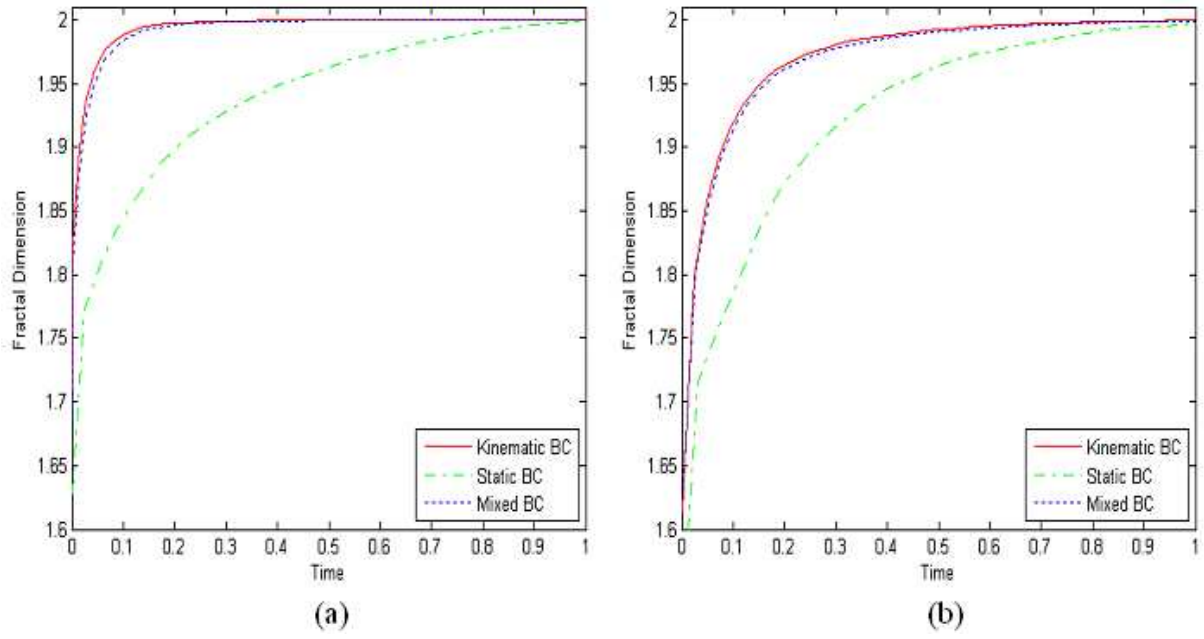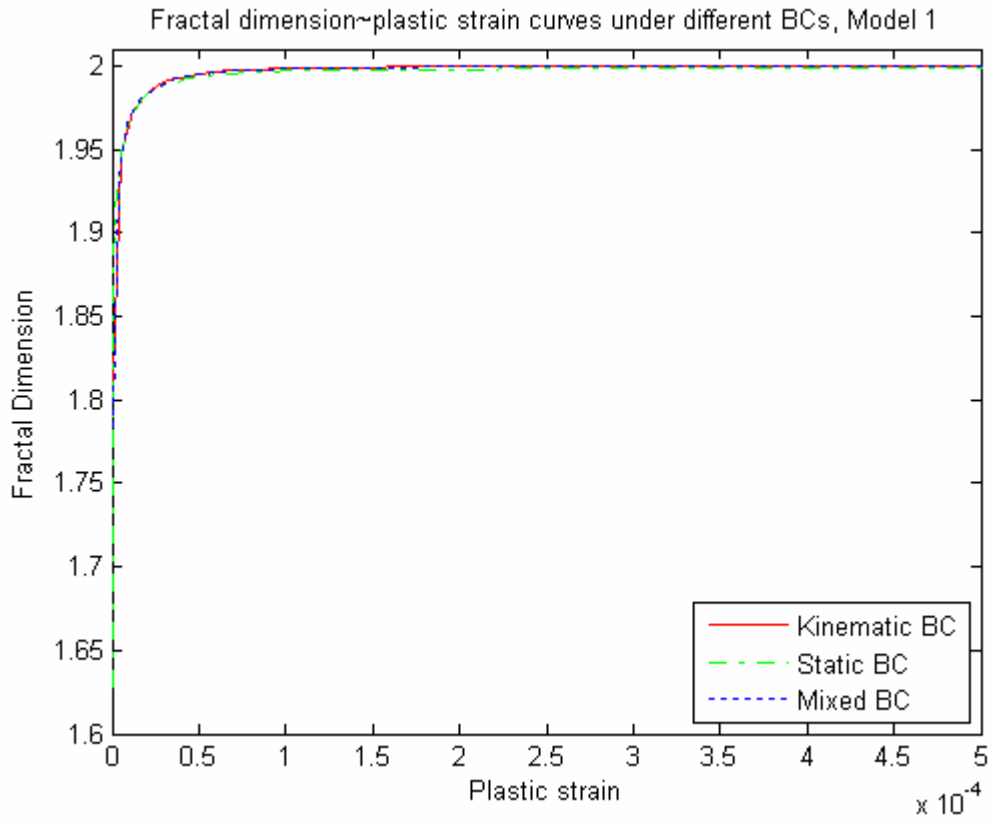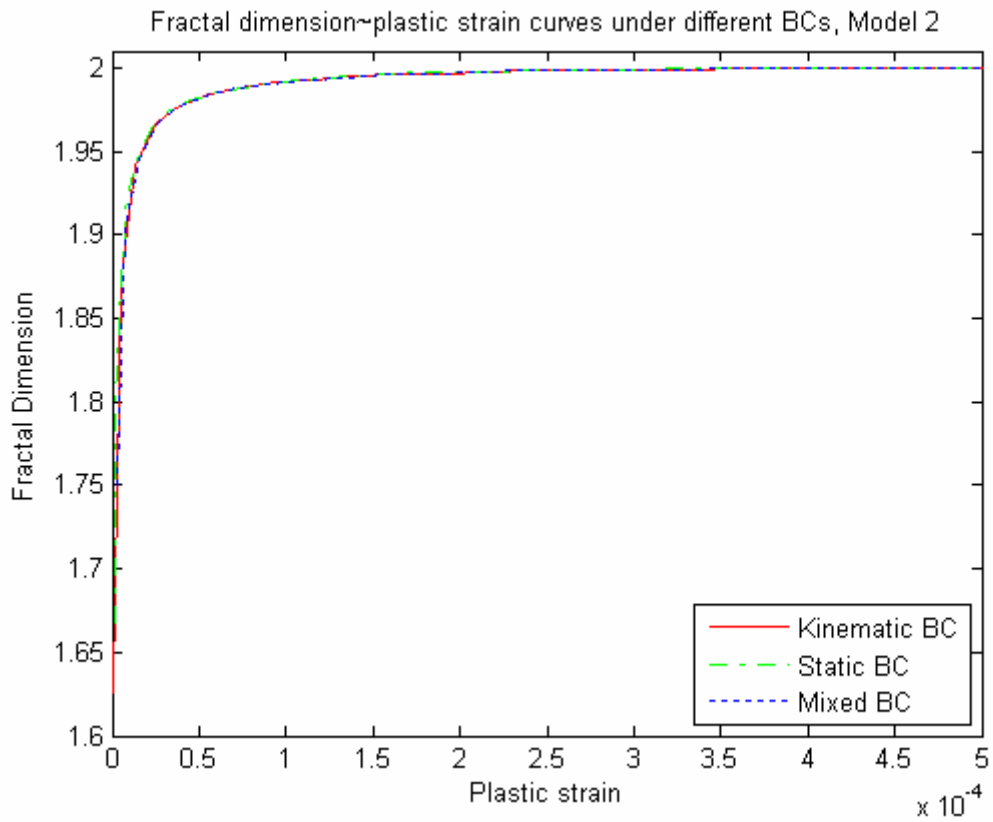
Figure 2.6: Time evolution curves of the fractal dimension under different BCs for: (a) model 1 (isotropic grains) and (b) model 2 (anisotropic grains). All loadings are linear in time.

(a)

(b)

Figure 2.7: Fractal dimension~plastic strain curves under different BCs for: (a) model 1 (isotropic grains) and (b) model 2 (anisotropic grains).
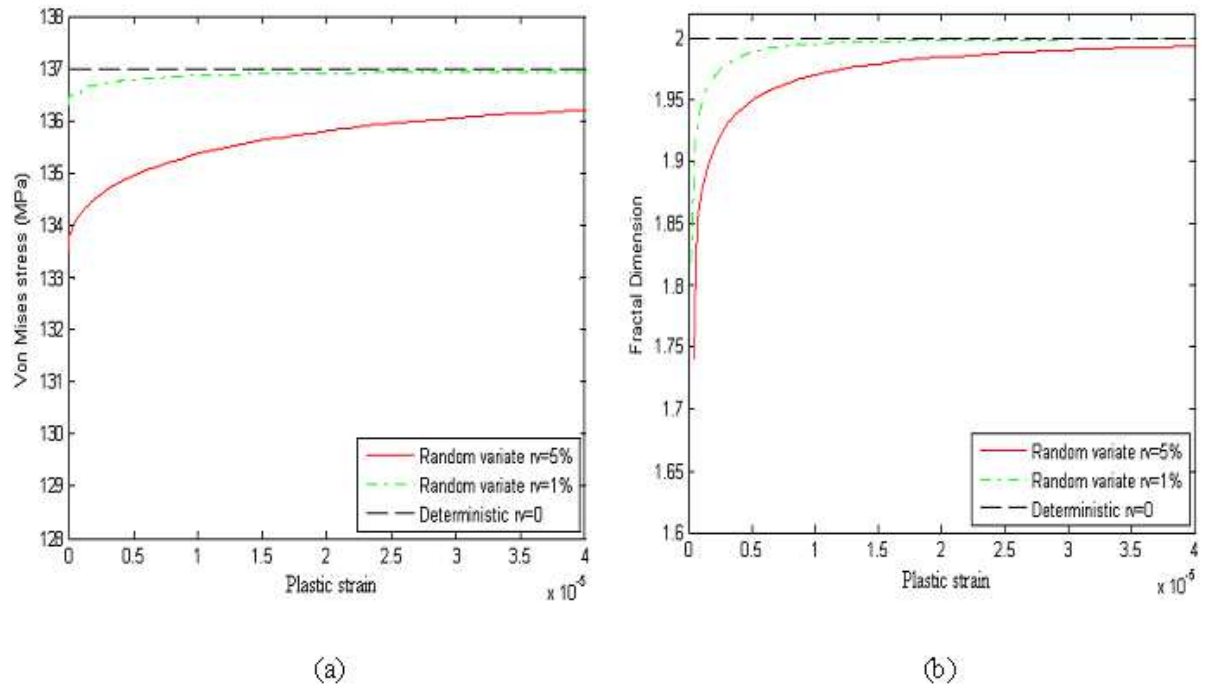
Figure 2.8: Comparison by different random variants (RV=5%, 1% and 0-deterministic case): (a) Average stress-strain curves and (b) Fractal dimension versus plastic strain.
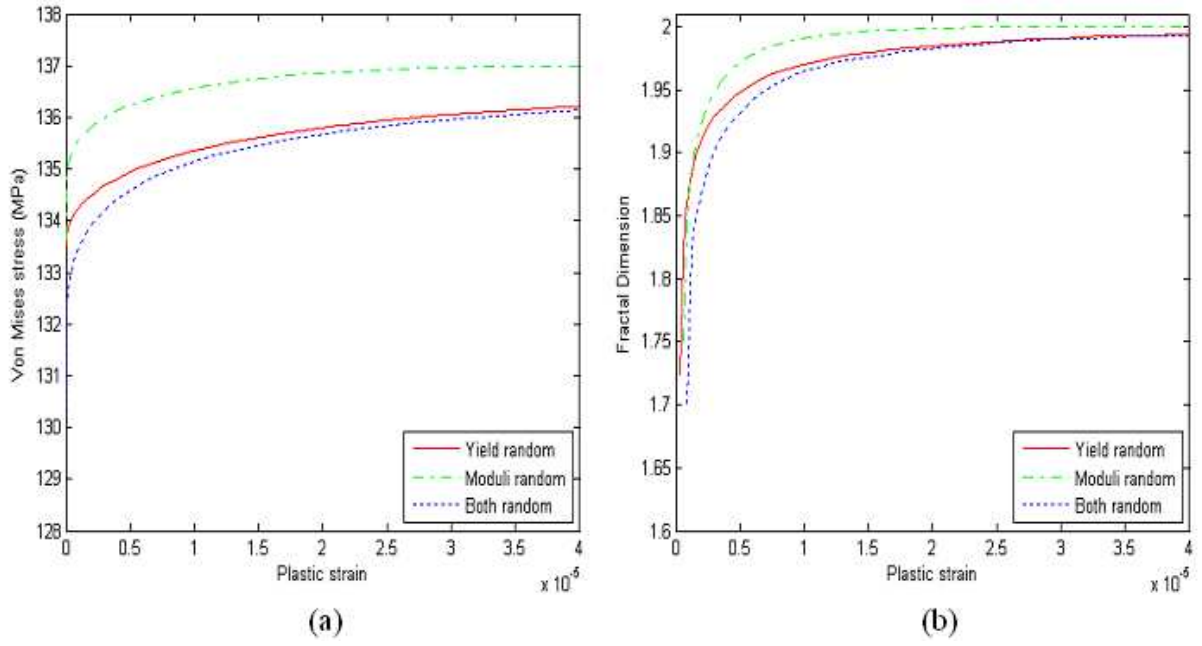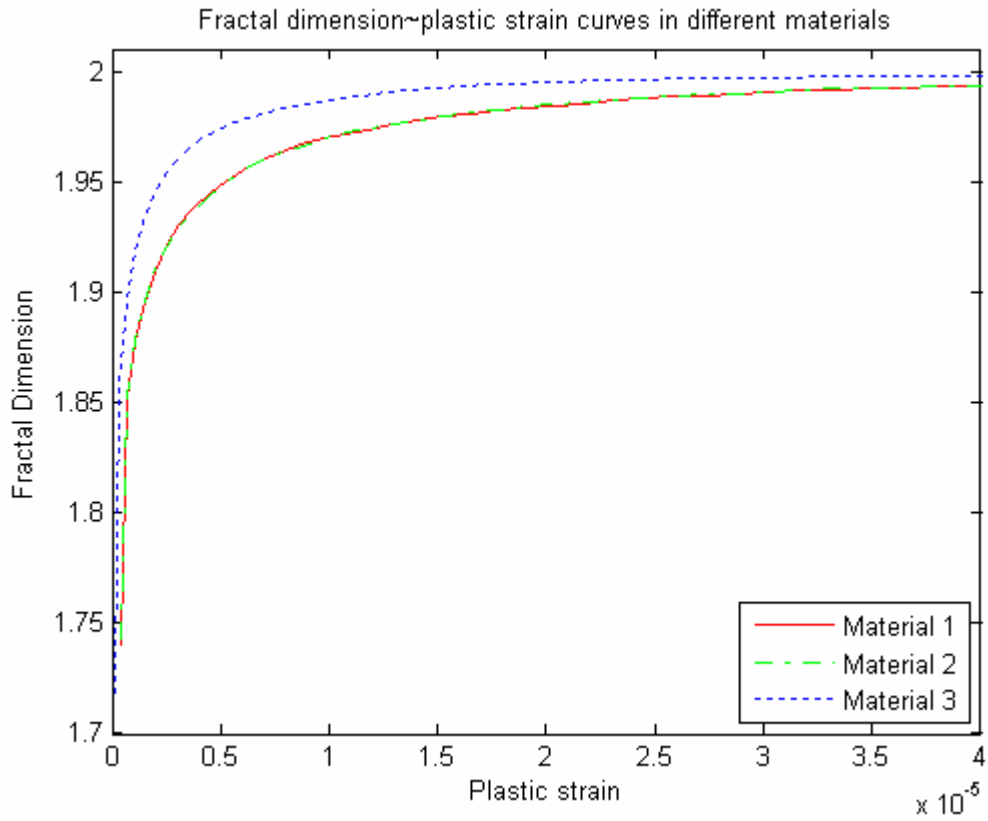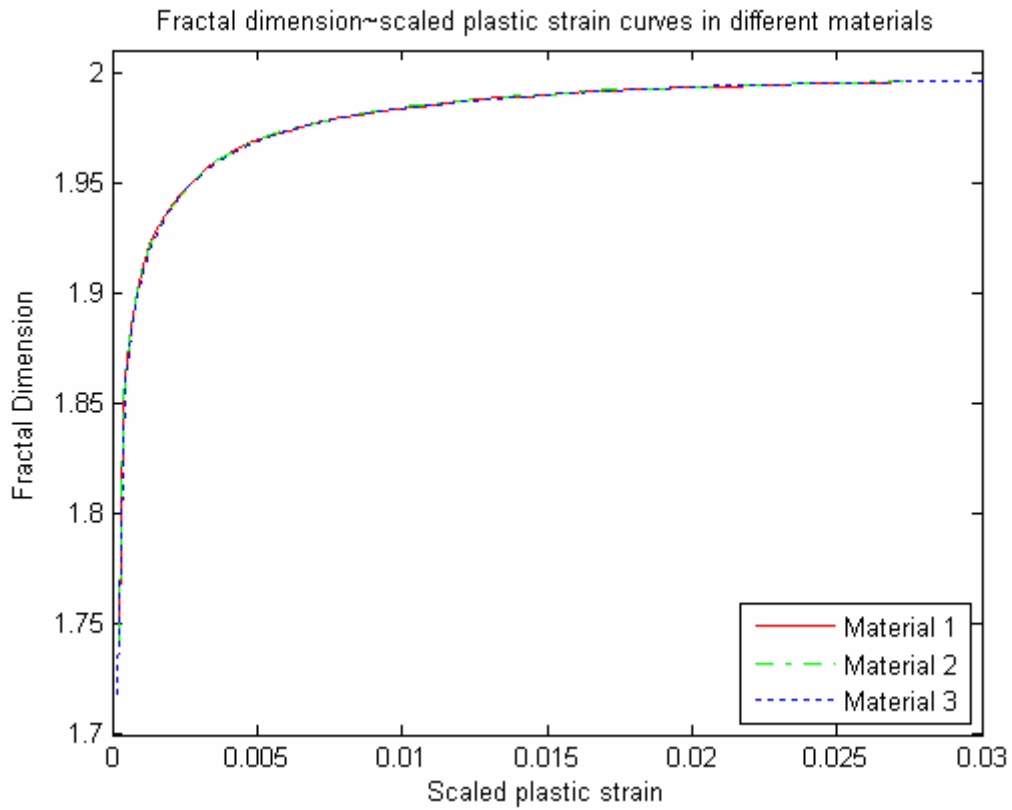
Figure 2.9: Comparison of the effects of random perturbations in the yield limit and/or elastic moduli: (a) average stress vs. average strain and (b) fractal dimension vs. plastic strain.

(a)

(b)

Figure 2.10: Comparison of different material responses: (a) Fractal dimension vs. plastic strain and (b) Fractal dimension vs. scaled plastic strain (i.e., scaled by yield strain).

CHAPTER 3

STUDY OF ELASTIC-HARDENING PLASTIC MATERIALS

In this chapter, we extend the study to more realistic model materials with elastic-hardening plastic, isotropic grains having random yield limits or elastic/plastic moduli. We focus on isotropic grains for simplicity and to see the hardening effects clearly. Following the set of grains that have become plastic, we find that it is still an evolving fractal monotonically plane-filling with an increasing macroscopic load. All these responses display smooth transitions but, as the randomness decreases to zero, they turn into sharp response of an idealized homogeneous material. The randomness in yield limits has a stronger effect than that in elastic/plastic moduli. In essence the hardening facilitates elastic-plastic transitions in random materials – larger plastic modulus leads to a faster transition. The fractal analysis methodology here implies a very practical application – the curves of fractal dimension versus applied stress display a universal character for a range of different materials – which offers a simple method of assessing the inelastic state of material. Finally, we give a qualitative explanation of the morphogenesis of fractal patterns from the standpoint of a correlated percolation on a Markov field on a graph network of grains[2].

3.1 Introduction

This chapter focuses on study of elastic-plastic transitions in elastic-hardening plastic materials, made of locally isotropic grains with random fluctuations in yield limits or elastic/plastic moduli. In particular, we pose the following questions as before: (1) Does the elastic-plastic transition occur as a fractal, plane-filling process of plastic zones under increasing, macroscopically uniform

---

[2] See also, [28] Li, J. and Ostoja-Starzewski, M., 2009. Fractals in elastic-hardening plastic materials, *Proc. R. Soc. A*, in press.

applied loading? (2) Is the fractal character of plastic zones robust under significant changes of material properties? (3) Can the fractal character of the set of plastic grains be explained through a stochastic model?

Motivated by these questions, a white-noise random microstructure is firstly set up, the key property of the model being that the material given *a priori* is non-fractal. Then, we determine fractal dimensions of sets of evolving plastic grains when the body is subjected to monotonic loading(s) consistent with the Hill-Mandel condition; several models and kinds of randomness are examined. Finally, we present a Markov field model of stochastic and fractal evolution of plastic grains, where the Markov property is dictated by the nearest-neighbor interactions between the contiguous grains.

3.2 Model formulation

A random heterogeneous material is defined as a set $\mathbf{B} = \{B(\omega); \omega \in \Omega\}$ of deterministic media $B(\omega)$, where ω indicates a specific realization and Ω is an underlying sample space [15]. The material parameters of any microstructure, such as the elasticity tensor or the yield tensor, jointly form a random field Θ which is required to be mean-ergodic on (very) large scales, that is

$$\overline{\mathbf{G}(\omega)} \equiv \lim_{L \to \infty} \frac{1}{V} \int_V \mathbf{G}(\omega, \mathbf{x}) dV = \int_\Omega \mathbf{G}(\omega, \mathbf{x}) dP(\omega) \equiv \langle \mathbf{G}(\mathbf{x}) \rangle \qquad (3.1)$$

We define a homogenized response as that in which there is equivalence between energetically ($\overline{\boldsymbol{\sigma} : \boldsymbol{\varepsilon}}$) and mechanically ($\overline{\boldsymbol{\sigma}} : \overline{\boldsymbol{\varepsilon}}$) defined effective responses $\overline{\boldsymbol{\sigma} : \boldsymbol{\varepsilon}} = \overline{\boldsymbol{\sigma}} : \overline{\boldsymbol{\varepsilon}}$. This is the well-known Hill-Mandel condition in linear elastic materials, leading to three types of uniform boundary conditions (BCs):

(1) kinematic (displacement) BC (with applied constant strain $\boldsymbol{\varepsilon}^0$):

$$\mathbf{u} = \boldsymbol{\varepsilon}^0 \cdot \mathbf{x}, \quad \forall \mathbf{x} \in \partial B_\delta; \qquad (3.2)$$

(2) traction (static) BC (with applied constant stress $\boldsymbol{\sigma}^0$):

$$\mathbf{t} = \boldsymbol{\sigma}^0 \cdot \mathbf{n}, \quad \forall \mathbf{x} \in \partial B_\delta; \tag{3.3}$$

(3) mixed-orthogonal (or displacement-traction) BC:

$$(\mathbf{t} - \boldsymbol{\sigma}^0 \cdot \mathbf{n}) \cdot (\mathbf{u} - \boldsymbol{\varepsilon}^0 \cdot \mathbf{x}) = 0, \quad \forall \mathbf{x} \in \partial B_\delta. \tag{3.4}$$

where $\mathbf{u}$ is the displacement vector and $\mathbf{t}$ is the traction vector on the specimen boundary ∂B_δ. The above boundary conditions can be generalized to elastic-plastic materials in an incremental setting [14,15]. The microstructures in our study are made of perfectly-bonded, homogeneous, isotropic grains of linear elastic/linear hardening-plastic (J_2) type with an associated flow rule [29]. Specifically, the constitutive response of any grain [i.e. a piecewise-constant region in a deterministic microstructure $B(\omega)$] is described by

$$d\varepsilon = \frac{3(1 - 2\nu)}{E} d\sigma \quad \left(d\varepsilon = \frac{d\varepsilon_{ii}}{3}, d\sigma = \frac{d\sigma_{ii}}{3} \right), \tag{3.5a}$$

$$d\varepsilon'_{ij} = \frac{1 + \nu}{E} d\sigma'_{ij} \quad \text{when } f < 0 \text{ or } df < 0, \tag{3.5b}$$

$$d\varepsilon'_{ij} = \frac{1 + \nu}{E} d\sigma'_{ij} + \lambda \cdot \frac{\partial f}{\partial \sigma'_{ij}} \quad \text{when } f \geq 0 \text{ and } df \geq 0. \tag{3.5c}$$

where primes indicate deviatoric tensor parts; E is the elastic modulus (Young's modulus), ν is the Poisson's ratio, and f is the yield function. (3.5b) indicates elastic deformation or plastic unloading and (3.5c) refers to plastic response. We consider the von Mises-Huber isotropic yield criterion and f is defined as

$$f = \sqrt{\frac{3}{2} \sigma'_{ij} \sigma'_{ij}} - c \tag{3.6}$$

Here c is the yield constant. In the 1D case the constitutive relations (3.5a-c) reduce to

$$\dot{\sigma} = E\dot{\varepsilon} \quad \text{when } \sigma < \sigma_s \tag{3.7a}$$

$$\dot{\sigma} = E_p \dot{\varepsilon}_p \quad \text{when } \sigma \geq \sigma_s \tag{3.7b}$$

Where σ_s is the yield stress in uniaxial tension ($= c\sqrt{3}$), ε_p is the plastic strain, and E_p is the plastic modulus. We can see that equations (3.7a-b) constitute a simple nonlinear model (piecewise-linear) characterizing the elastoplastic response. Figure 3.l shows such a homogeneous body

transitioning instantaneously from elastic (white) to plastic (black) state, accompanied by a kink in the stress-strain curve.

3.3 Simulations of fractal patterns of plastic grains

3.3.1 Evolutions of fractal patterns

We consider 2D plane strain problem and apply shear loading through one of the three types of uniform BCs consistent with (3.2)-(3.4):

$$
\begin{aligned}
&\text{Kinematic: } \varepsilon_{11}^0 = -\varepsilon_{22}^0 = \varepsilon, \ \varepsilon_{12}^0 = 0, \\
&\text{Mixed: } \varepsilon_{11}^0 = \varepsilon, \sigma_{22}^0 = -\sigma, \varepsilon_{12}^0 = \sigma_{12}^0 = 0 \\
&\text{Traction: } \sigma_{11}^0 = -\sigma_{22}^0 = \sigma, \ \sigma_{12}^0 = 0,
\end{aligned}
\tag{3.8}
$$

A computational mechanics study is conducted with an FEM commercial software ABAQUS [23]. We take a sufficiently large domain comprising 256×256 square-shaped grains. Each individual grain is homogeneous and isotropic, its E, E_p being constant and σ_s being a field of independent identically distributed (i.i.d.) uniform random variables scattered up to $\pm 2.5\%$ about the mean. Other kinds of randomness are studied in Section 3.3.3. The material constants are taken from ABAQUS 6.8 Benchmarks 3.2.1 case 1:

$$E = 68.94 \, GPa, E_p = 34.47 \, GPa, \sigma_s = 68.94 \, MPa, \upsilon = 0.3.$$

Figures 3.2(a-d) show elastic-plastic transition fields at different deformation stages under traction BC. We follow here the binary format of Fig. 3.1 in the sense that elastic (plastic) grains are white (black). The plastic grains form plastic regions of various shapes and sizes, and we estimate the fractal dimension D of that entire plastic grain set by using a "box-counting method" [26]:

$$D = -\frac{\log(N_r)}{\log(r)} \tag{3.9}$$

where Nr denotes the number of boxes of size r needed to cover the object. Results of box counts

for Figs. 3.2(a-d) are shown in Figs. 3.3(a-d), respectively. With the correlation coefficients of log(Nr) versus log(r) close to 1.0 for all black-white patterns, we conclude that the elastic-plastic transition patterns are fractal. Note the orthotropic character of the plastic grain set, which reflects the propensity of shear bands and slip-lines to form approximately at $\pm 45^{o}$.

Figures 3.4(a,b) show response curves under these three BCs in terms of the averaged stress *vs.* strain and the fractal dimension (D) *vs.* strain, respectively. The responses of single grain homogeneous phases are also given for a reference. In both figures, the curves overlap, demonstrating that the (256×256) domain is the Representative Volume Element (RVE). Here we assign each grain with one finite element for convenience. To verify whether such a meshing is sufficient, we conduct numerical simulations using different element types (linear or quadric) and illustrate the results in Figs. 3.5(a,b). Clearly, the curves are nearly identical. Thus, the 256×256 domain size is chosen so as to ensure the RVE level response and computational accuracy, while having an acceptable spatial resolution of dependent fields to ensure a reliable assessment of fractal dimensions.

3.3.2 Discussion of hardening effects

In order to investigate the influence of hardening in the transition, we conduct comparison studies among different materials with various plastic modulus and/or yield strain (σ_s / E). Their material parameters are listed in Table 3.1, with Poisson's ratio being 0.3 in all the cases. Here we note that materials 1 and 2 are taken from ABAQUS 6.8 Benchmarks 3.2.1 case 1 and 2, respectively, while the materials 3a and 3b are designated to be different in yield strain from materials 1 and 2; their parameters E, σ_s are those of 316 steel in ABAQUS 6.8 Example Problems 1.1.8. The series A materials (2a,3a) have the same ratio of plastic-to-elastic modulus, E_p / E, as the material 1, while series B materials (2b,3b) are the same in their plastic modulus E_p. The compared responses are considered in terms of dimensionless quantities like normalized

stress or strain (rescaled by yield stress or yield strain) accordingly.

We begin the discussion by comparing responses of material 1 and 2. As seen from Table 3.1, these materials have the same yield strain but very different hardening parameters E_p. Note that the hardening constant of material 2 is much less than that of material 1, we see from Fig. 3.6(a) that the tendency of approaching a homogeneous response in material 2 is slower than that in material 1. Accordingly, the fractal dimension grows slower in material 2 as observed in Fig. 3.6(b), which means that the elastic-plastic transition develops more rapidly in materials with stronger hardening effects.

Note that materials 1 and 2 also differ much by elastic modulus. To see the hardening effects more clearly, we perform numerical simulations on two hypothetical materials 2a, 2b—the former with same E_p / E of material 1 while for the latter same in E_p. The results are given in Fig. 3.7 for comparison. We observe that responses of materials 1 and 2a are nearly identical in the curves of both, the normalized stress-strain and the fractal dimension-strain. While for material 2b with the same E_p of material 1 but a lower E_p / E, the tendency of approaching the homogeneous response appears slower and the same conclusions can be drawn regarding the fractal dimension curves.

While the study of materials 1 and 2 (Figs. 3.6a,b) has been restricted to cases in the same yield strain, we now turn to materials with different yield strains. This is done by comparisons of material 1 and other two hypothetical materials 3a, 3b—same configurations of E_p / E or E_p but different in yield strain. The results are illustrated in Fig. 3.8. We arrive at the same conclusions as for materials 2a and 2b. Based on these observations, we conclude that the elastic-plastic transition in random materials is characterized by their fractal dimension-normalized plastic strain responses. Specifically, the same response curves in fractal dimension-normalized plastic strain results in the same normalized stress-strain relations. The hardening effect is fully determined by the ratio of plastic-to-elastic modulus, E_p / E. The same E_p / E leads to the same fractal

transition patterns, and the larger is E_p / E the faster is the increase of fractal dimensions, i.e. the hardening facilitates the elastic-plastic transition in random materials.

While our study is restricted to linear hardening materials, a simple extension to nonlinear hardening models can also be drawn here—for those cases the hardening parameter E_p is not a constant but some function with regard to the state of plastic strain, and the ratio E_p / E can be specified in each incremental step during the transition. We note that, in conventional stress-strain calibrations, the trends to approach homogeneous response curves are not easy to discern among different materials. On the other hand, the fractal dimension always increases from 0 to 2 during the transition, thus providing an optimal parameter to assess the transition process.

3.3.3 Other types of randomness

Now, we examine the influence of material parameter randomness. This is again studied through comparisons of several cases. As suggested in Section 3.3.2, we consider the response curves in terms of fractal dimension versus normalized plastic strain. First, the sensitivity of transition processes to material's model randomness is investigated in two scenarios:

Scenario A: Scalar random field of the yield limit, with three types of randomness:

A1 - Yield limit is a uniform random variable up to $\pm2.5\%$ about the mean.

A2 - Yield limit is a uniform random variable up to $\pm0.5\%$ about the mean.

A3 - Deterministic case: no randomness in the yield limit.

Scenario B: Random field of the yield limit or elastic modulus, with two cases:

B1 = A1.

B2 – Elastic modulus is a uniform random variable up to $\pm2.5\%$ about the mean.

Results for A1-A3 and B1-B2 are shown in Figs. 3.9 and 3.10, respectively. From Fig. 3.9 one can conclude that different random variables in the model configuration lead to different transition processes; overall, a lower randomness results in a faster elastic-plastic transition. Next,

in Fig. 3.10 we observe the randomness in yield limits to have a stronger effect than that in elastic modulus.

Note that the hardening parameter (plastic modulus E_p) can also be randomly perturbed. In fact, it is more realistic to combine the randomness in elastic modulus and plastic modulus in applications of composites of various material constitutes. We conduct this study through a comparison of three cases:

Case 1: B2, the plastic modulus is fixed.

Case 2: Elastic modulus is a uniform random variable up to $\pm 2.5\%$ about the mean, while the plastic modulus is a corresponding linearly dependent random variable: E_p / E is fixed.

Case 3: Elastic modulus and plastic modulus are i.i.d. uniform random variables up to $\pm 2.5\%$ about the mean.

Figure 3.11 illustrates the results for these cases. We can find that the three curves are practically overlapping, which means that the randomness in plastic modulus has a very small effect in the transition.

3.3.4 Further discussions

In Sections 3.3.1-3.3.3, we have demonstrated that the set of all plastic grains at the elastic-plastic transition is an evolving fractal, and studied hardening effects and material model randomness appealing to the fractal dimension. While the fractal dimension versus normalized plastic strain curves prove effective in comparing transition patterns among different materials, we note that the fractal dimension always reaches 2.0 in the end of the transition, which hints at a universal property for all elastic-plastic materials. To demonstrate this clearly, we plot the curves of fractal dimension versus normalized Mises stress for materials 1, 2b and 3b in Fig. 3.12(a). We choose these three materials as in Section 3.3.2, and their fractal dimension~normalized plastic strain curves are different. Interestingly, from Fig. 3.12(a), it appears that the curves are nearly

identical for all these materials.

One may argue that a simple variable like the volume fraction of plastic regions could also describe the transition, since it reaches 1.0 in the fully developed stage. Accordingly we plot the results of plastic volume fraction versus normalized Mises stress in Fig. 3.12(b). Although the responses of materials 2b and 3b nearly overlap (in effect the E_p / E ratios are very close), they differ from material 1. This leads us to conclude that the relation between D and the normalized Mises stress is a universal property (or at least varies very little) for all isotropic elastic-plastic hardening materials. Since the fractal dimension can readily be estimated via, say, image analysis, this provides an effective approach to infer the stress in the material at the transtion.

3.4 Why are fractals observed in elastic-plastic materials?

The fractal character of evolving sets of plastic grains observed in computational mechanics simulations reported above may be explained by a reference to fractals on Markov random fields (MRF). To see this, we first introduce a binary random variable S describing the state of any grain as

$$S = \begin{cases} e & \text{if} \;\; f_p < 0 \;\; \text{or} \;\; df_p < 0, \\ p & \text{if} \;\; f_p \geq 0 \;\; \text{and} \;\; df_p \geq 0. \end{cases} \tag{3.10}$$

where e means an elastic state and p means a plastic state. f_p refers to the yield function of grain p. Next, consider grain centers of our polycrystal as a Cartesian lattice $\mathbb{Z}^2$ of spacing a in $\mathbb{R}^2$, that is

$$L_a = \left\{ \mathbf{x} = \left(m_1 a, m_2 a \right) \right\}, \tag{3.11}$$

where m_1, m_2 are integers ranging from 1 through N $(= 256$ in our simulations above). Given that (i) the properties (yield stresses or elastic/plastic modulus) of each grain is random, and (ii) the state of each grain is a result of all the interactions in the entire system of all grains, the state S on L_a is a random field

$$S : \Omega \times L_a \rightarrow \{e,\, p\}, \; S(\omega, \mathbf{x}) = e \; \text{ or } \; p. \tag{3.12}$$

In other words, for any $\omega \in \Omega$ (a particular realization of the entire material system) and any location $\mathbf{x}$ on the lattice, the state S is s (i.e., either e or p). If we do not specify $\mathbf{x}$, then s stands for a realization $S(\omega) = s$ on L_a, where some grains are elastic and others plastic. Note that the body is subjected to a macroscopic load: either $\boldsymbol{\varepsilon}^0$ or $\boldsymbol{\sigma}^0$, according to BCs (3.2) or (3.3).

Markov property: Recognize that, given the macroscopic load such as $\boldsymbol{\varepsilon}^0$, the conditional probability of a grain at $\mathbf{x}$ being plastic at any macroscopic load level depends not on the state of all other grains $L_a - \{\mathbf{x}\}$ but only on the state of its *nearest neighborhood* $N_\mathbf{x}$:

$$P_{\boldsymbol{\varepsilon}^0}\left\{ s(\mathbf{x}) \,|\, s(N_\mathbf{x}) \right\} = P_{\boldsymbol{\varepsilon}^0}\left\{ s(\mathbf{x}) \,|\, s(L_a - \{\mathbf{x}\}) \right\}. \tag{3.13}$$

This relation defines S of (3.13) as a *Markov random field* (MRF). Given the square lattice topology of our composites, $N_\mathbf{x}$ comprises four neighboring grains:

$$N_\mathbf{x} = \left\{ \mathbf{x} = \left[(m_1+1)a, m_2 a \right], \left[(m_1-1)a, m_2 a \right], \left[m_1 a, (m_2+1)a \right], \left[m_1 a, (m_2-1)a \right] \right\},$$

$$\tag{3.14}$$

whereby we consider the effect of four grains acting through the vertices onto $\mathbf{x}$ as being much weaker than those which contact through the sides. Since this accounts for neighbors just one step away, S is called a *1-Markov field*. It is understood, but not written explicitly in (3.13), that the conditional probabilities on both sides of that equation depend on the macroscopic applied loading, i.e. $\boldsymbol{\varepsilon}^0$ or $\boldsymbol{\sigma}^0$ or some combination thereof, applied, respectively, through (3.2) - (3.4).

Note that the nearest neighborhood may be replaced by a set of neighbors up to two steps away (in Manhattan metric), whereby S would be a *2-Markov field*. This would lead to a richer model, but we do not need to pursue it here, because already the 1-Markov field possesses the salient features of a correlated percolation.

The formulation above is analogous to that of an MRF for an Ising magnet on a square lattice, where the state (spin up or down) of each site is a function of the spins at four neighboring sites

and of the overall temperature T (rather than that of a mechanical state)

$$P_T \{s(\mathbf{x}) \mid s(N_\mathbf{x})\} = P_T \{s(\mathbf{x}) \mid s(L_a - \{\mathbf{x}\})\}. \tag{3.15}$$

The temperature does also appear when one writes a Gibbs specification of the random field:

$$\Pi_T (\omega) = \frac{1}{Z} \exp[-U(\omega, T)]. \tag{3.16}$$

This is called a *Gibbs random field* (GRF), with Z being a partition function ensuring the probability measure is normalized to 1:

$$Z = \sum_\omega \exp[-U(\omega, T)]. \tag{3.17}$$

Going back to the elasto-plastic composite, instead of (3.16), we can also write a Gibbs specification

$$\Pi_{\varepsilon^0}(\omega) = \frac{1}{Z} \exp[-U(\omega, \varepsilon^0)]. \tag{3.18}$$

Now, the equations (3.16) and (3.18) also betray the second reason for the formulation above to be analogous to the MRF for an Ising magnet. Namely, the internal energy of the latter is $U(\omega, T)$, while the internal energy of the MRF of an elastic-plastic composite is $U(\omega, \varepsilon^0)$. This is consistent with a continuum thermomechanics picture where the temperature is a control parameter for a thermal problem, while strain is a control parameter for a mechanical problem.

It is well known that every MRF is equivalent to a GRF, and *vice versa* [30]. However, the key issue that arises is whether the description in terms of conditional probabilities $P_{\varepsilon^0}\{s(\mathbf{x}) \mid s(N_\mathbf{x})\}$ is equivalent to the description in terms of absolute probabilities $\Pi_{\varepsilon^0}(\omega)$. That is, if we specify a MRF in terms of local interactions, do we also specify its probability measure Π (and, therefore, its state ω) in a unique way? The answer to this question depends on whether the interactions are weak or strong. When they are weak in the sense that the state $s(\mathbf{x})$ depends weakly on the neighbors' states $s(N_\mathbf{x})$, then there is a unique correspondence between $P_{\varepsilon^0}\{s(\mathbf{x}) \mid s(N_\mathbf{x})\}$ and $\Pi_{\varepsilon^0}(\omega)$. On the other hand, when they are strong (in the sense of strong such dependence), for a given specification of interactions $P_{\varepsilon^0}\{s(\mathbf{x}) \mid s(N_\mathbf{x})\}$ there is

more than one probability measure $\Pi_{\varepsilon^0}(\omega)$. The critical point where this non-uniqueness occurs is characterized by fractal patterns.

In the case of the Ising model, this critical point is the Curie point T_C on the temperature scale, below which we have a ferromagnet, and above which there is a spatial disorder of spins so that no single dominant (and hence macroscopic) spin emerges. A wide range of binary patterns — i.e., white (W) versus black (B) vertices — have been analyzed for the entire range of control parameters [31]. The control parameters are α (the likelihood of any single vertex to co-align with the external magnetic field) and β (the strength of interaction), so that a canonical form of the internal energy reads

$$U(\omega,T) = \alpha|V_B| + \beta|V_{BW}| \tag{3.19}$$

where $|V_B|$ is the number of black vertices, and $|V_{BW}|$ is the number of pairs having one black and one white vertex.

Note that the first term in (3.19) here is responsible for a Bernoulli type (i.e. uncorrelated) percolation on the lattice. While this percolation — i.e. retaining only the first term in (3.19) — is well known to also exhibit fractal patterns, the mechanics and physics considerations suggest that the second term is non-zero, so the elastic-plastic transition is characterized by a correlated percolation. In fact, for a weakly random microstructure, the plastic state is likely to 'spill over' to a neighboring elastic grain. On the other hand, in a strongly random microstructure, plasticity tends to go via weak grains around grains with high yield limits [24]. Thus, in some cases the interactions may be attractive, and in others repulsive. Note that (i) the correlated percolation involves an interplay of both terms in (3.19), and (ii) the problem being tensorial in nature and orthotropic, it is more complex than what happens on the Ising model which is only scalar.

In the early eighties fractals were hardly known and this is probably why [31] did not estimate fractal dimensions from their computer simulations, although fractal patterns are clearly seen in their figures at (and around) T_C. The task of generating fractal patterns via MRF models

and computing their fractal dimensions was accomplished by [32] and followed by others in the field of image analysis, e.g. [33].

Returning back to our elastic-plastic transition in a random composite we recapitulate:

(i) there are elastic (*e*) and plastic (*p*) vertices in analogy to *W* and *B* vertices in the Ising model;

(ii) the increasing applied loading ε^0 tends to cause the $e \rightarrow p$ transition at any single vertex, while the local conditioning is attractive in the sense that *p* states on $N_\mathbf{x}$ tend to make $S(\mathbf{x}) = p$ (with the same cause-effect relation holding for *e*);

(iii) *S* is the MRF so that the evolution of the entire *V* set from a predominantly *e* state to a predominantly *p* state exhibits fractal patterns.

Since the responses under (3.2) and (3.3) loadings have been shown to be almost the same (i.e. the RVE level), the above arguments could be restated with ε^0 replaced by σ^0. While this section provides only a qualitative explanation of the morphogenesis of fractal patterns at elastic-plastic transitions, a quantitative determination of conditional probabilities of the MRF is outside the present study.

3.5 Summary

We study evolving sets of plastic grains at elastic-plastic transitions in several random 2D plane strain material models. In particular, these are composites of linear elastic/hardening plastic, isotropic grains having fluctuations in yield limits or elastic/plastic moduli, which are taken as strict-sense white-noise (non-fractal) random fields. It turns out that in every model material subjected to increasing uniform loading (either kinematic, traction or mixed) the sets of evolving plastic grains are fractal, with the fractal dimension growing from 0 in the globally elastic state to 2 in a globally plastic state. Several models and kinds of randomness are examined, always displaying the same essential features. We find that the transition is characterized thoroughly by

the ratio of plastic-to-elastic moduli – the larger the ratio, the faster the transition, i.e., the hardening effect indeed facilitates the transition process. Also, as the random field noise vanishes, the transition from elastic to plastic occurs instantaneously (i.e. D goes from 0 to 2 discontinuously), whereby the smooth response curve of the random composite turns into a stress-strain curve with a kink. The model comprising many subdomains with random material properties generates an overall smooth transition which is physically more feasible. This study has a very practical application: the curves of fractal dimension versus applied stress – which indeed unifies responses for a range of different materials – provides a simple approach to infer the stress in materials at transitions.

Table 3.1: Material parameters

Material	1	2	2a	2b	3a	3b
$E\ [GPa]$	68.94	207	207	207	192	192
$E_p\ [GPa]$	34.47	10.41	103.5	34.47	96	34.47
$\sigma_s\ [MPa]$	68.94	207	207	207	120	120
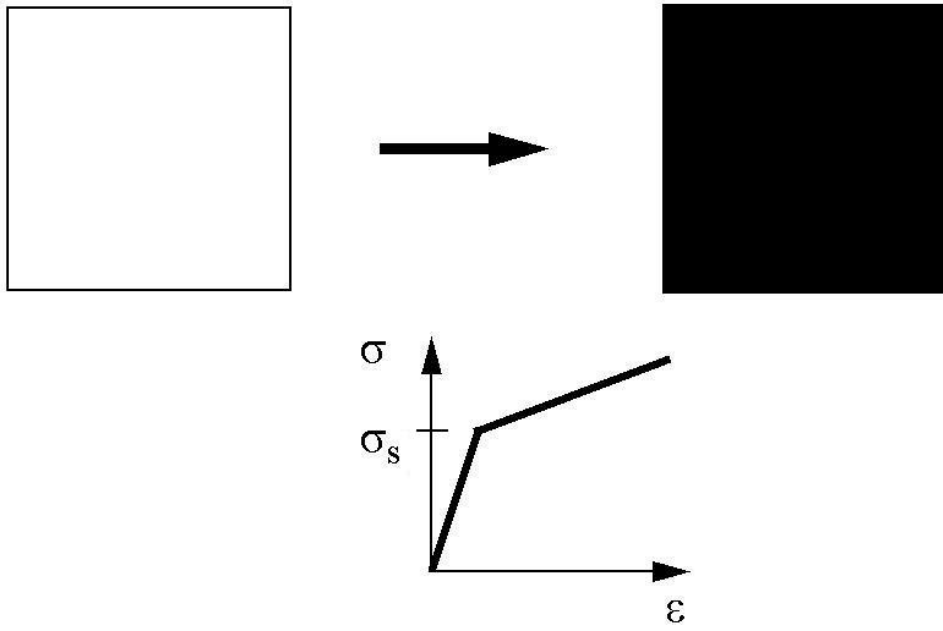
Figure 3.1: Elastic-plastic transition in an ideal, homogeneous body is reflected in an instantaneous change from elastic (white) to plastic (black) and a kink in the stress-strain curve.
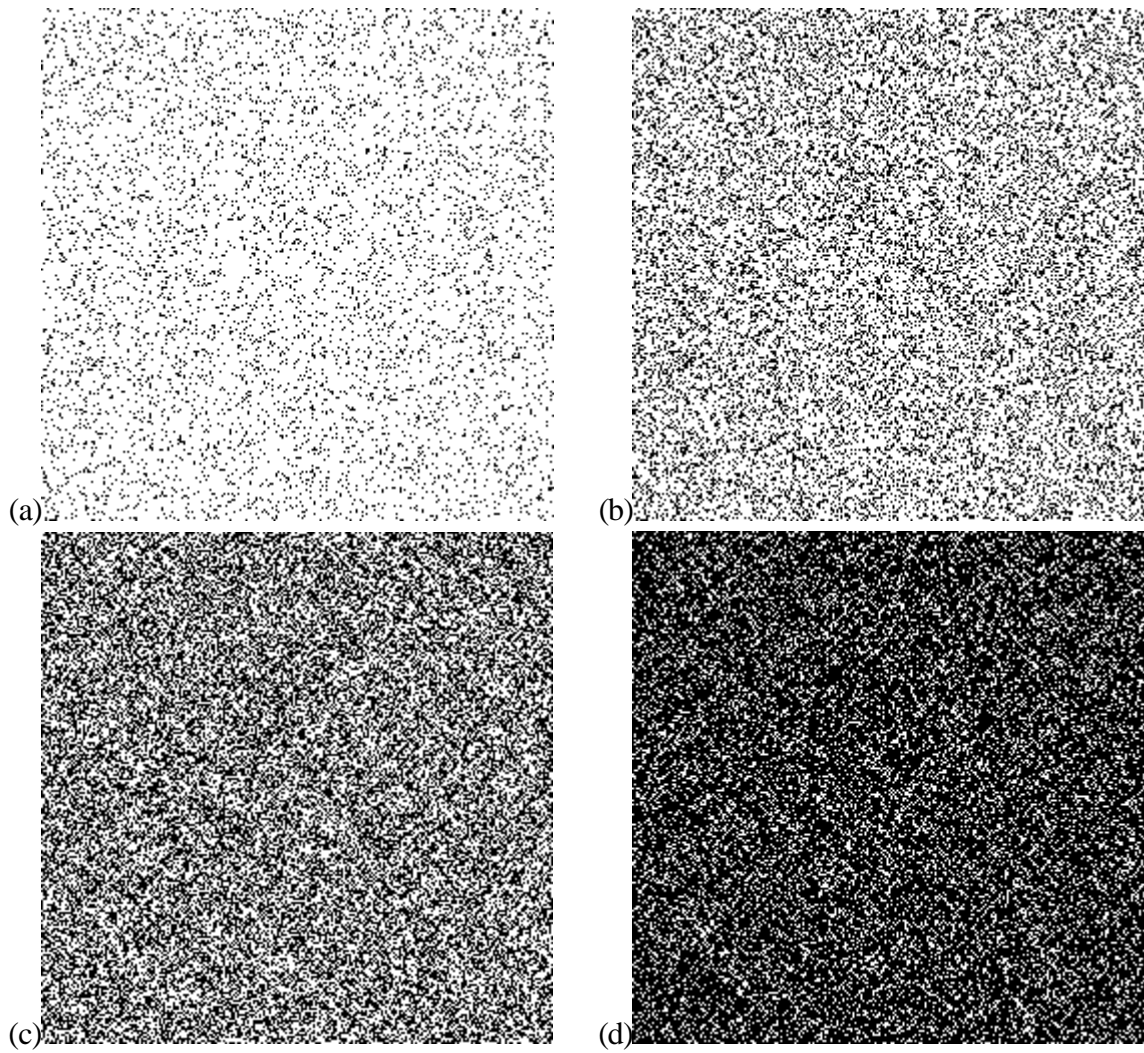
Figure 3.2: Field images (white: elastic; black: plastic) at four consecutive stress levels applied to a material with weak randomness in the yield limit via uniform traction BCs. The average plastic strain (a) 1×10^{-7}; (b) 1×10^{-6}; (c) 4×10^{-6}; (d) 1×10^{-5}.
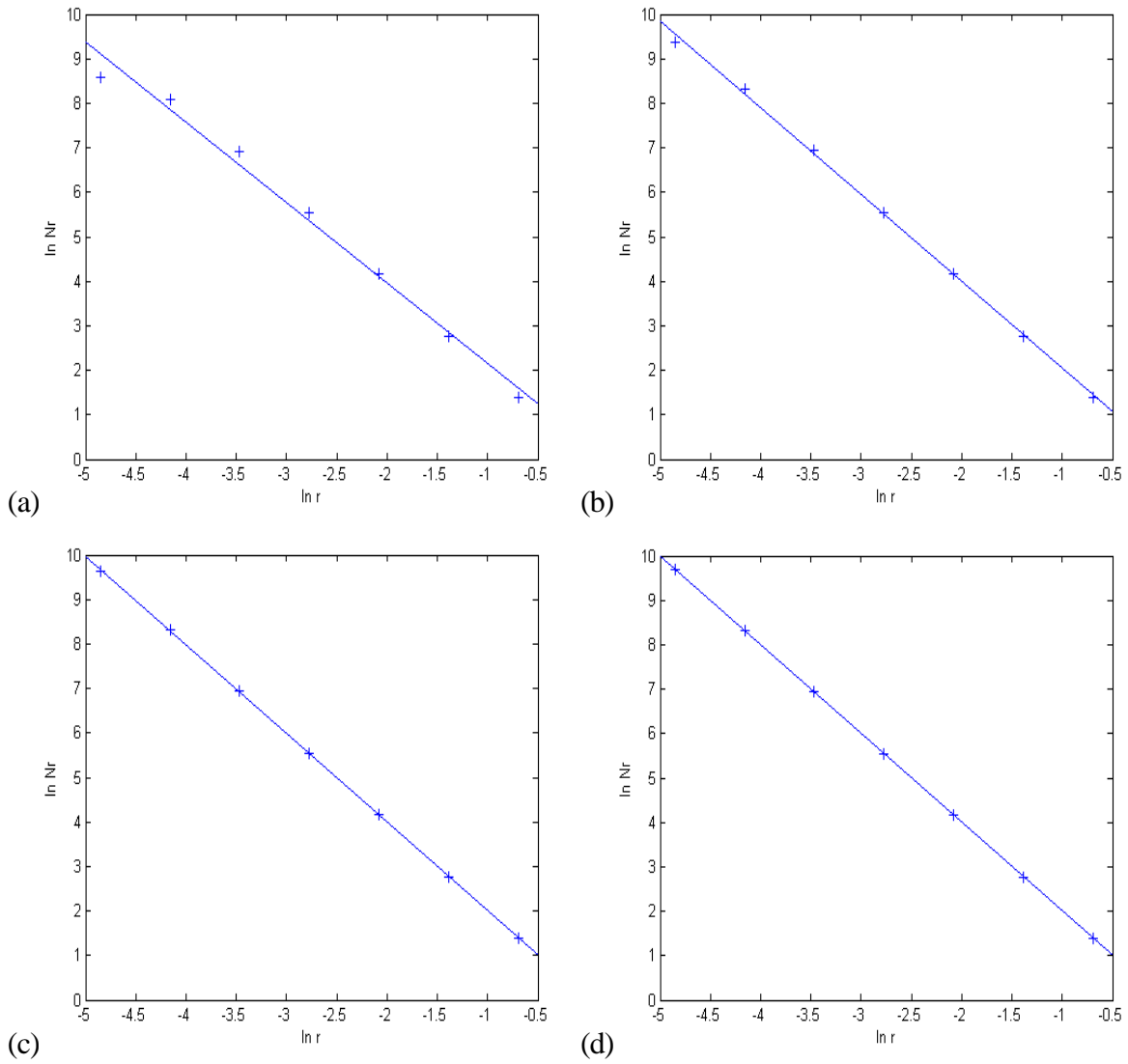
Figure 3.3: Estimation of the fractal dimension *D* for Figs. 3.2(a-d), respectively, using the box-counting method: (a) *D*=1.8012; (b) *D*=1.9591; (c) *D*=1.9914; (d) *D*=1.9996. The lines correspond to the best linear fitting of *ln*(*Nr*) vs. *ln*(*r*).
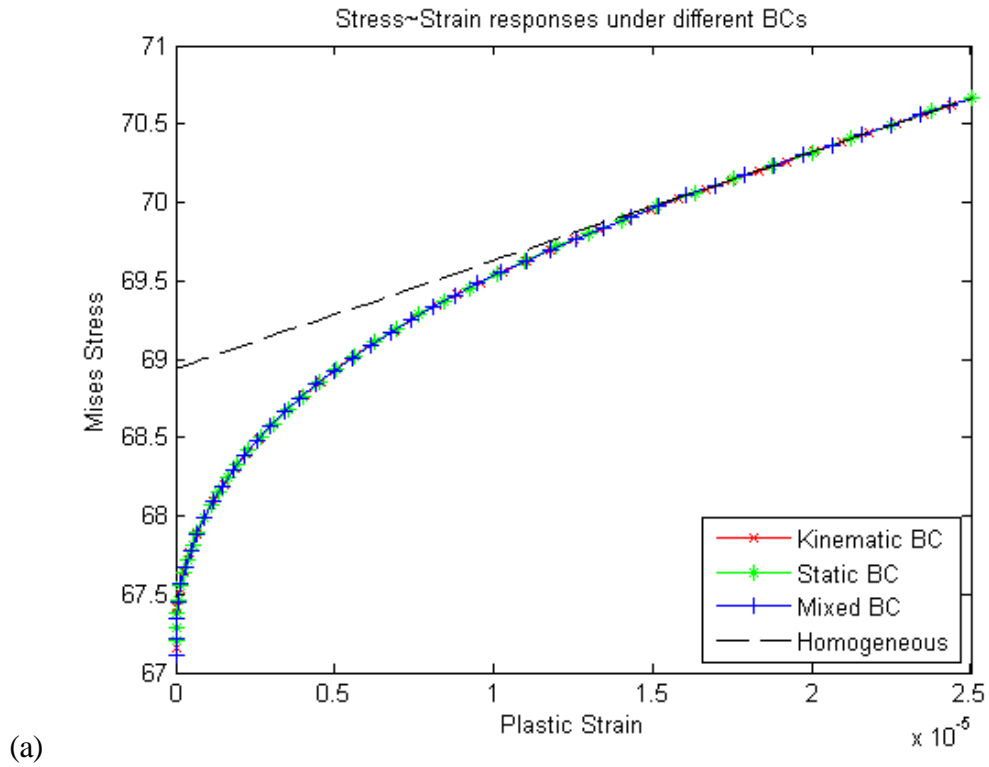
(a)
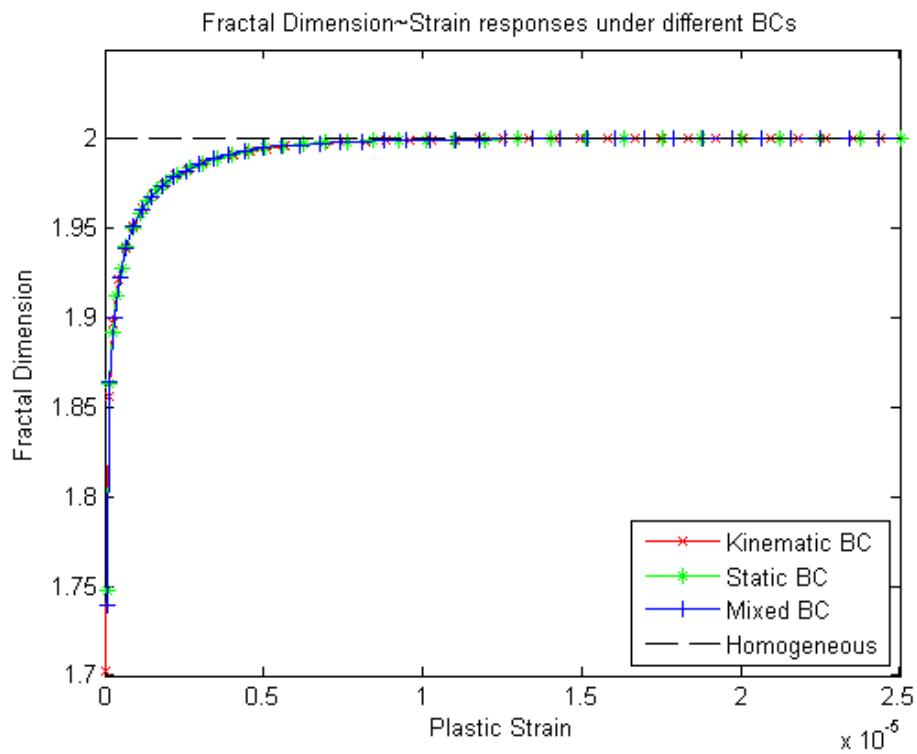
(b)

Figure 3.4: Response curves for the material of Figs. 3.2 and 3.3 under different boundary conditions: (a) Volume averaged stress versus strain; (b) Fractal dimension versus strain.

(a)

(b)
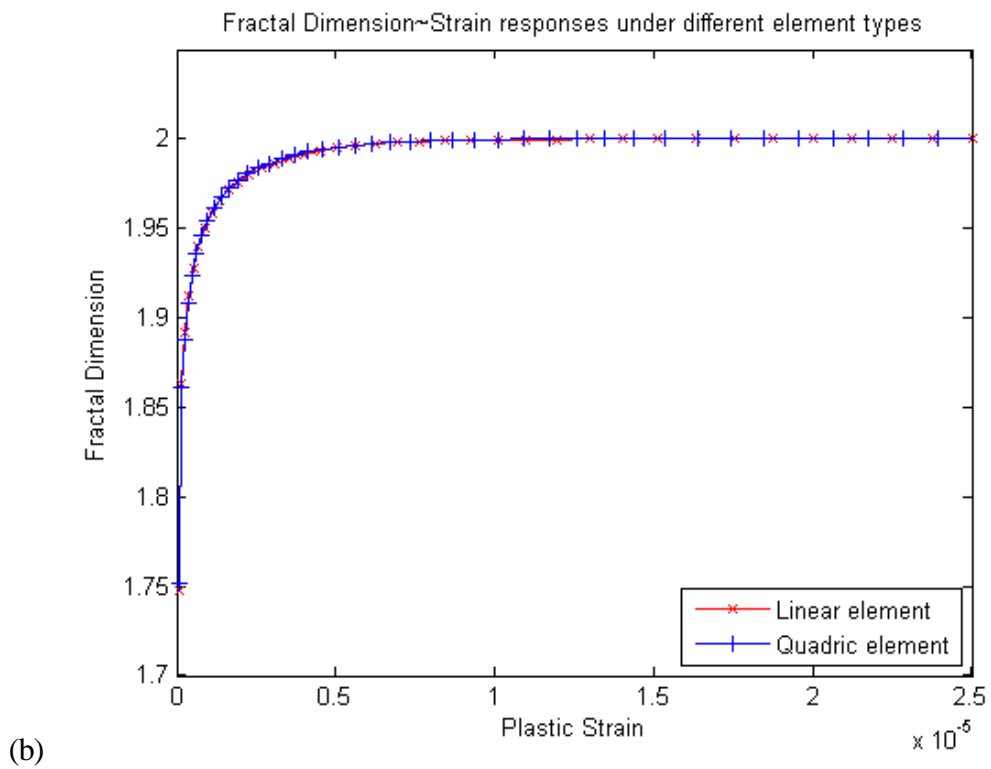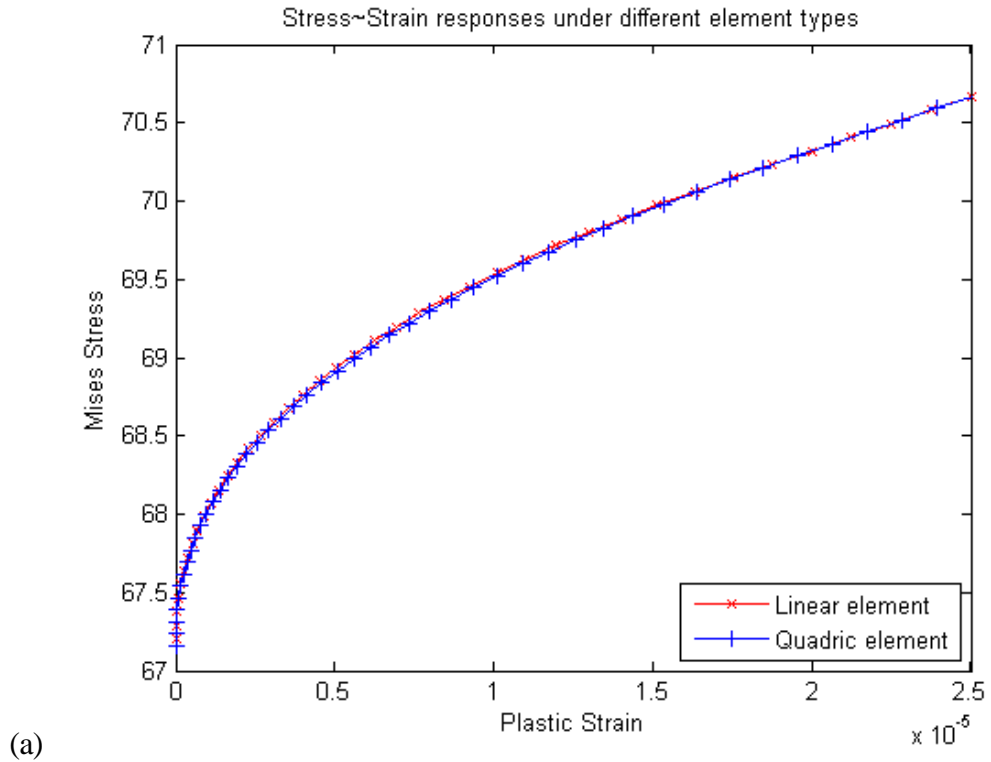
Figure 3.5: Response curves under different finite element types: (a) Volume averaged stress versus strain; (b) Fractal dimension versus strain.
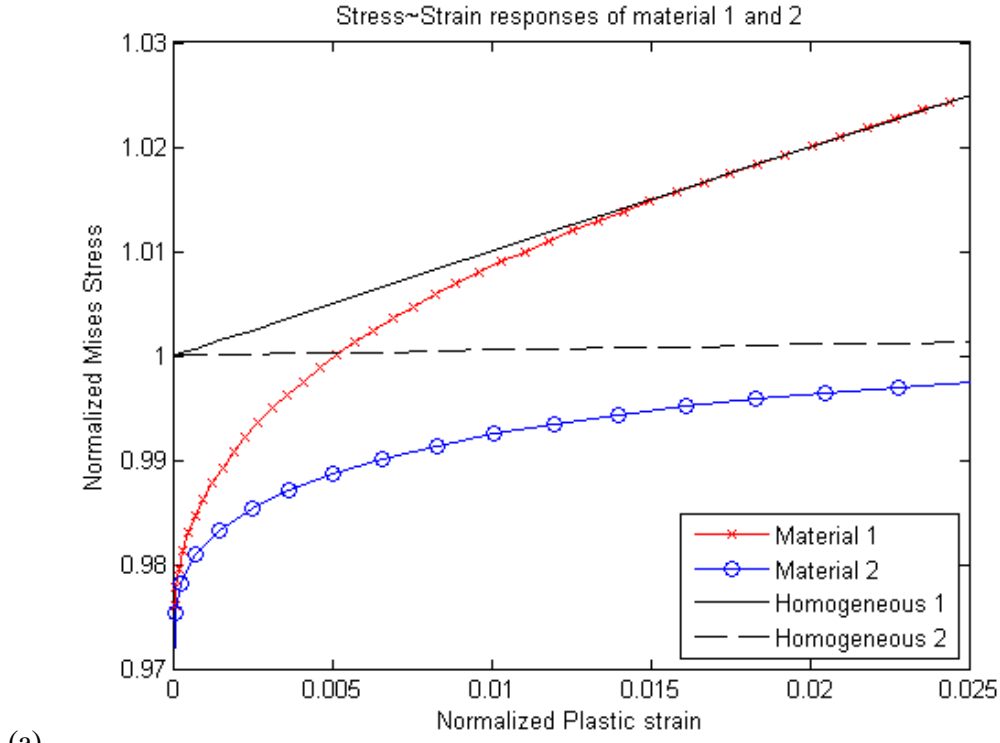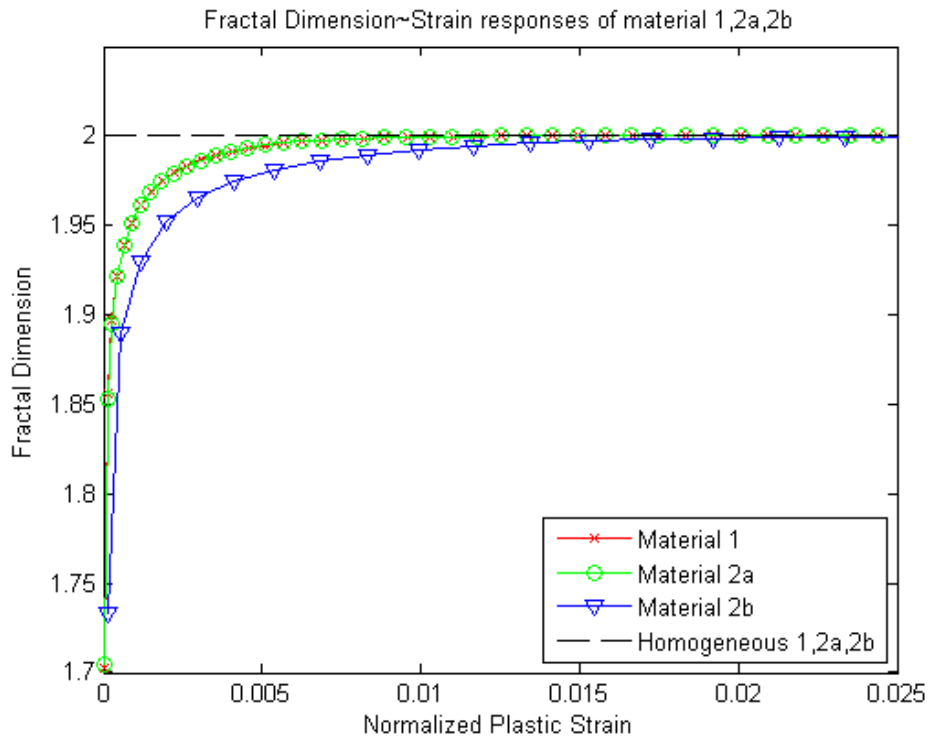
(a)
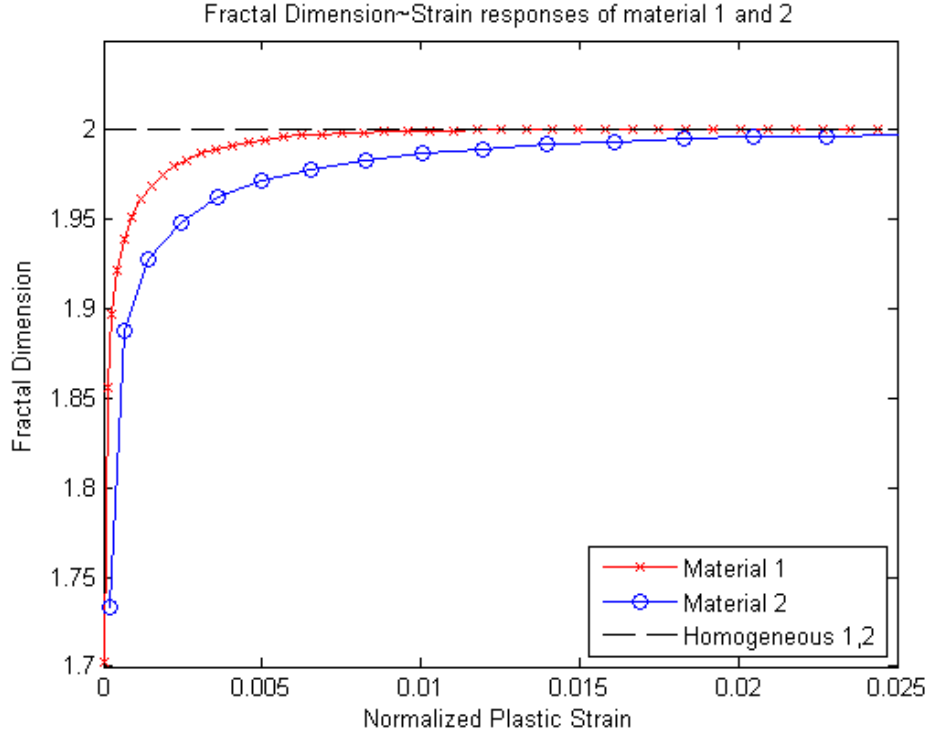
(b)

Figure 3.6: Comparison of Material 1 and 2: (a) Volume averaged stress versus strain; (b) Fractal dimension versus strain.
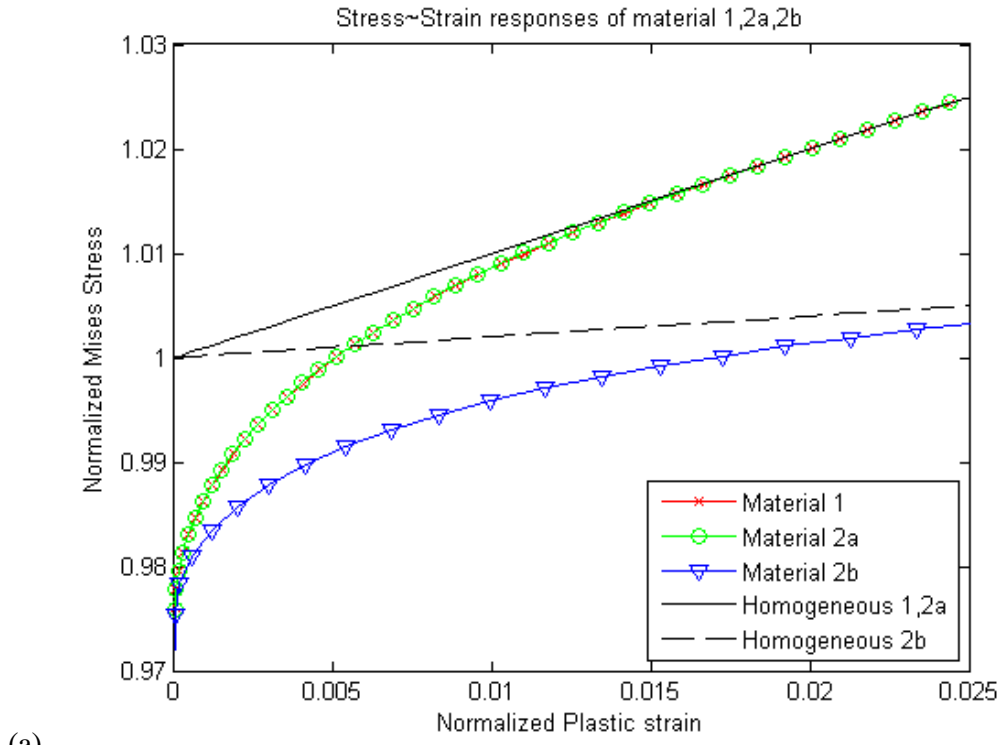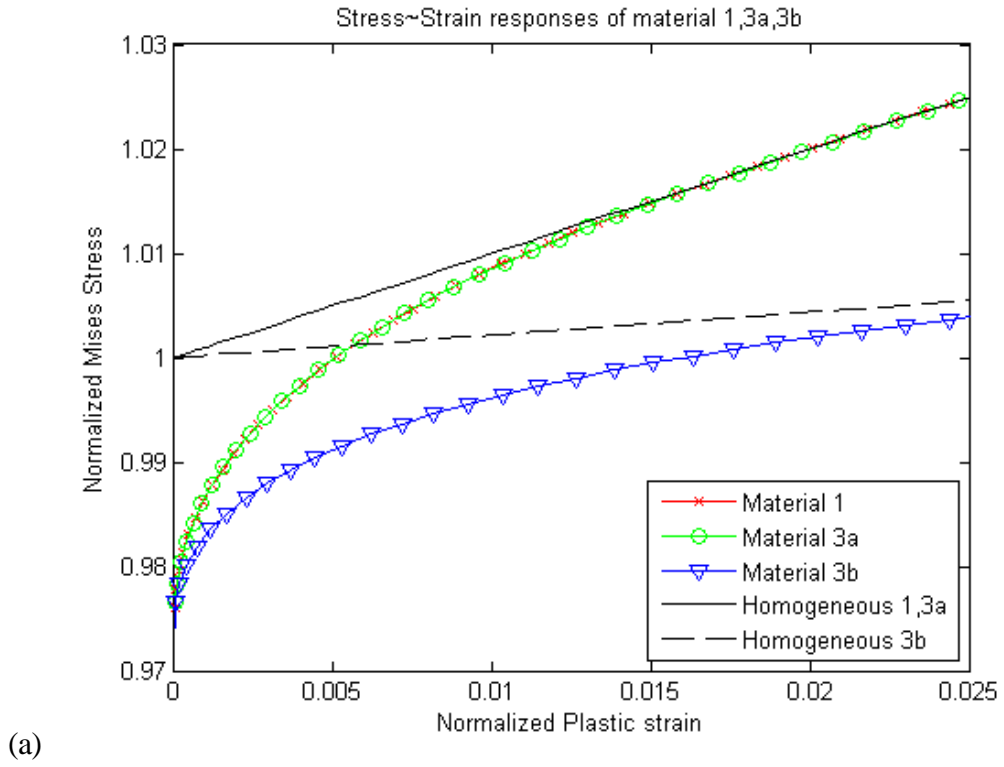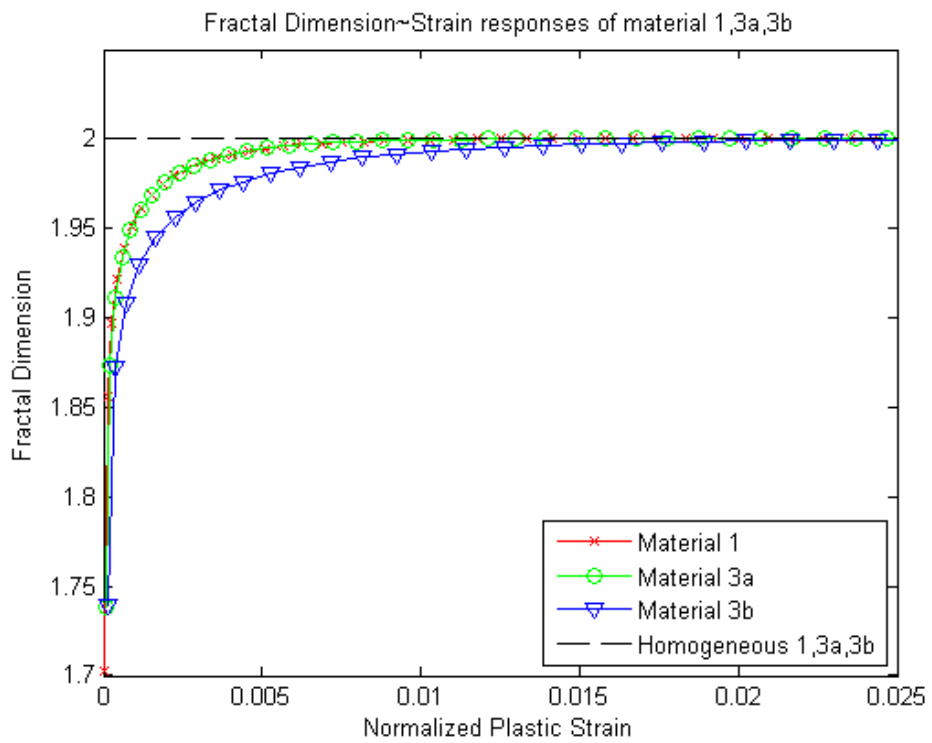
(a)

(b)

Figure 3.7: Comparison of material 1 and 2a, 2b: (a) Volume averaged stress versus strain; (b) Fractal dimension versus strain.

(a)

(b)

Figure 3.8: Comparison of material 1 and 3a, 3b: (a) Volume averaged stress versus strain; (b) Fractal dimension versus strain.
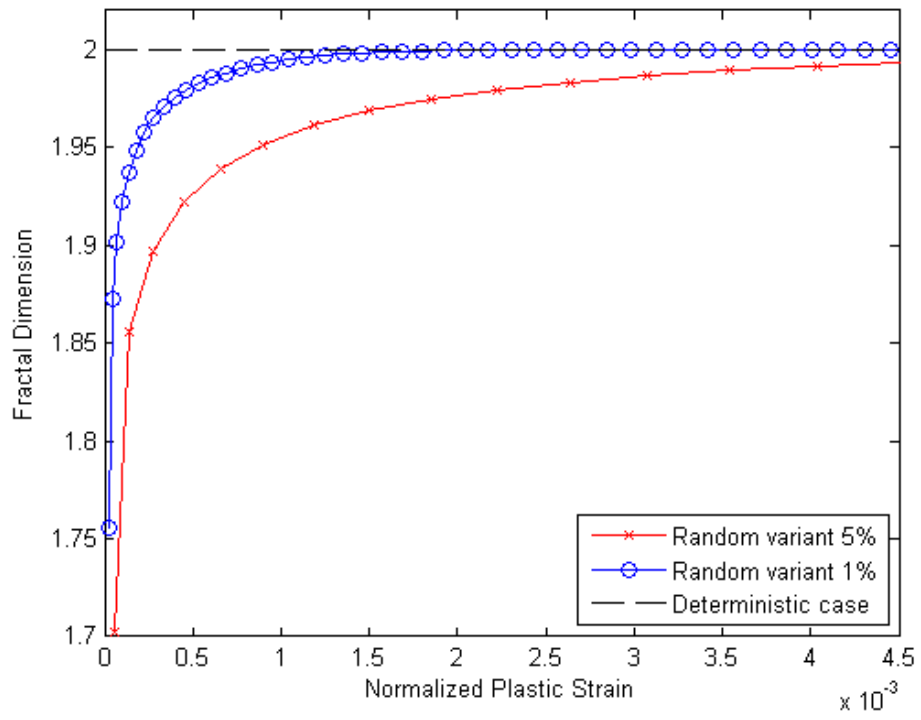
Figure 3.9: Comparison by different random variants: RV=5%, 1% and 0-deterministic case.
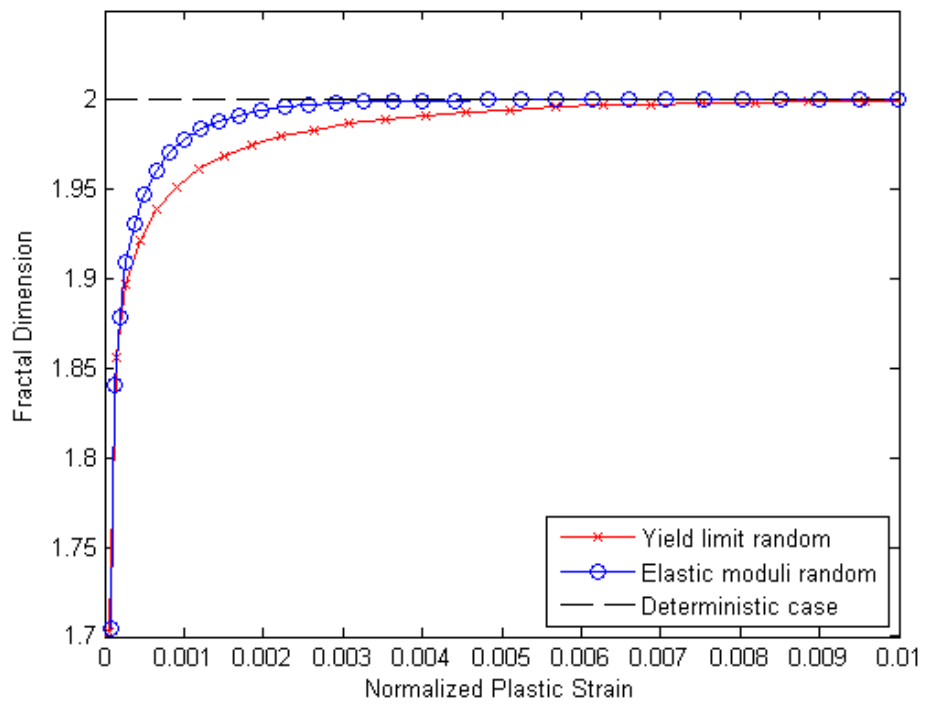
Figure 3.10: Comparison of the effects of random perturbations in the yield limit or elastic moduli.
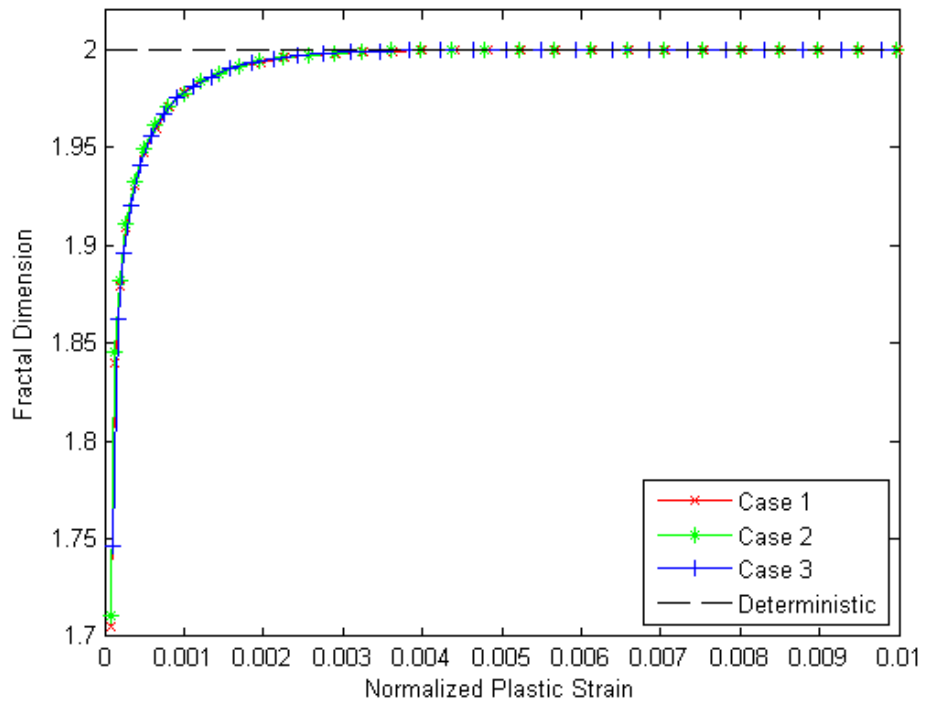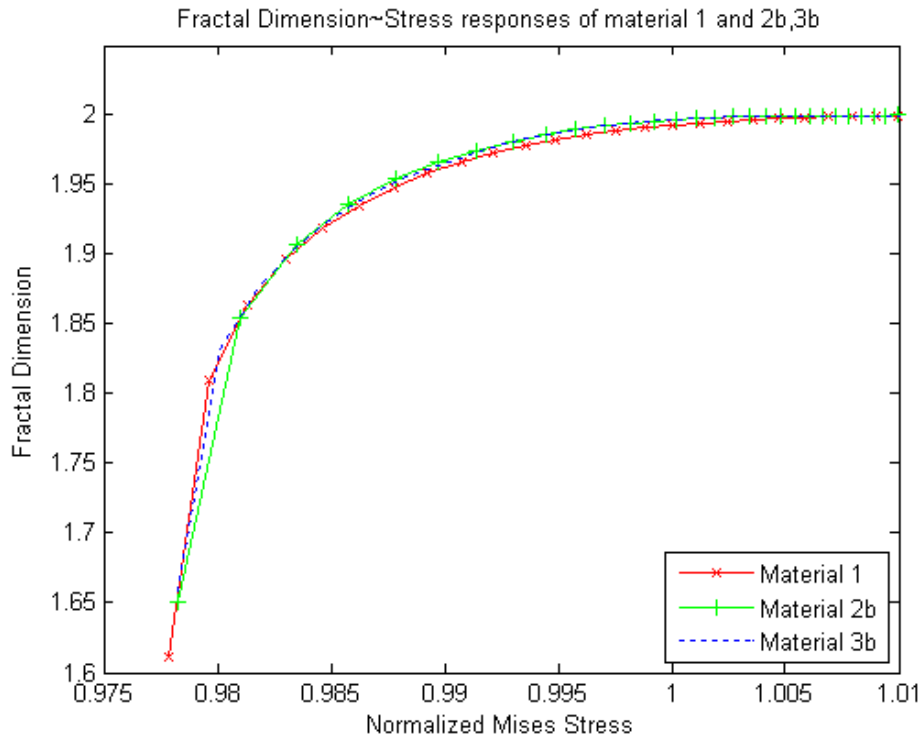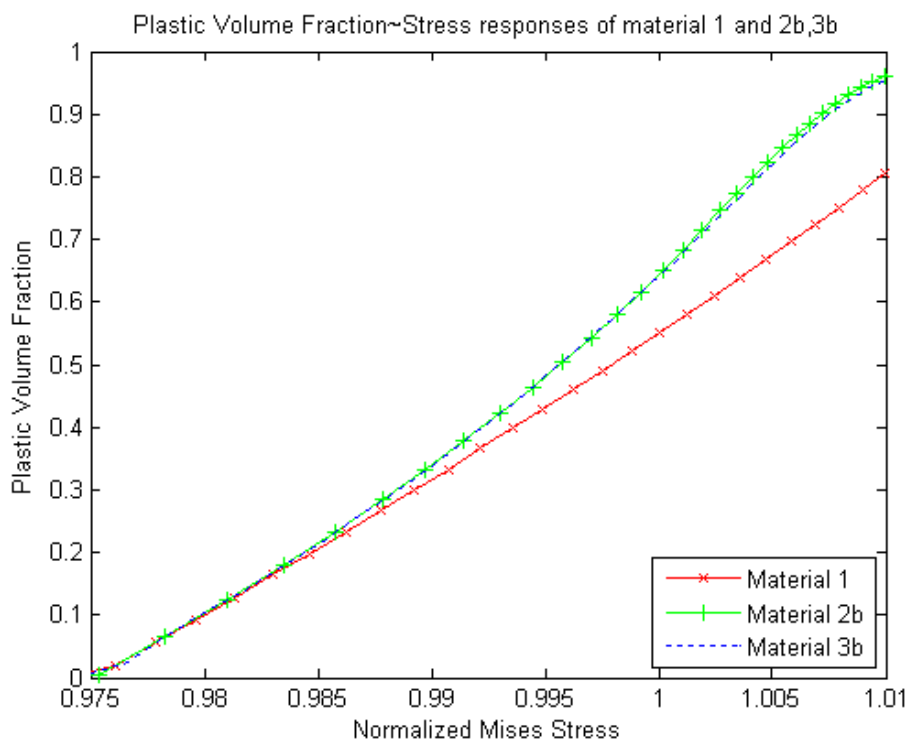
Figure 3.11: Comparison of the effects of random perturbations in plastic modulus: Case 1- plastic modulus fixed; Case 2-plastic modulus and elastic modulus linear dependent; Case 3-plastic modulus and elastic modulus independent.

(a)

(b)

Figure 3.12: Response curves among material 1 and 2b, 3b: (a) Fractal dimension versus stress; (b) Plastic volume fraction versus stress.

CHAPTER 4

FRACTALS IN THERMO ELASTIC-PLASTIC MATERIALS

This chapter is a continuation of the work following fractals in elastic-plastic transitions. After discussing cases of elastic-perfectly plastic and elastic-hardening plastic media, now we turn to more general situations – random thermo elastic-plastic materials (or elastic-plastic type with residual strains). The model is comprised of locally homogeneous isotropic grains with weak random fluctuations in either the moduli, or plastic limits, or thermal expansion coefficients. We first focus on the case of random perturbated thermal expansion coefficients (or residual strains) and find that the set of plastic grains is a continually evolving, and ultimately plane-filling, fractal structure. On the other hand, the complementary set – elastic grains – is still a fractal but with its dimension decreasing from 2 to 0. Furthermore, the comparison study under various model randomness and material constants is conducted to demonstrate thermal elastic and hardening plastic effects altogether in elastic-plastic transitions. It turns out that the fractal dimension D is an optimal parameter of describing the transition patterns in a unified way for a range of all different materials[3].

4.1 Model formulation

As conventionally done in mechanics of random materials, we consider the random heterogeneous material to be a set $\mathcal{B} = \{B(\omega); \omega \in \Omega\}$ of realizations $B(\omega)$, defined over the sample space Ω, each one evolving in a deterministic fashion [15]. That is, for an elementary event $\omega \in \Omega$ we

---

[3] See also, [34] Li, J. and Ostoja-Starzewski, M., 2009. Fractal pattern formation in thermoelastic-plastic, heterogeneous materials. *Proceedings of the 8th International Congress on Thermal Stresses,* 283-286.

have a realization of deterministic media $B(\omega)$, each taken as an aggregate of crystals (or grains). With $\mathcal{B}$ embedded in a physical space, the aggregate is essentially modeled by a random field. The random field of any material property $\mathbf{G}$ is required to be mean-ergodic, that is

$$\overline{\mathbf{G}(\omega)} \equiv \lim_{L \to \infty} \frac{1}{V} \int_V \mathbf{G}(\omega, \mathbf{x}) dV = \int_\Omega \mathbf{G}(\omega, \mathbf{x}) dP(\omega) \equiv \langle \mathbf{G}(\mathbf{x}) \rangle \tag{4.1}$$

where the overbar means the volume average and $\langle \ \rangle$ indicates the ensemble average. In general, the grains are homogeneous, isotropic, linear thermoelastic-hardening plastic materials, where the randomness resides in either the moduli, or plastic limits, or thermal expansion coefficients. Now we focus on the case of random thermal expansion coefficients. Thus, the constitutive response of each grain is written as

-when $f < c$ (thermoelastic region)

$$\varepsilon_{ij} = S_{ijkl} \sigma_{kl} + \alpha_{ij}(\omega, \mathbf{x})\theta \tag{4.2}$$

-when $f \geq c$ (plastic region)

$$d\varepsilon_{ij}' = \frac{d\sigma_{ij}'}{2G} + \lambda \cdot \frac{\partial f}{\partial \sigma_{ij}}$$

$$d\varepsilon = \frac{d\sigma}{K} \left(d\varepsilon = \frac{d\varepsilon_{ii}}{3}, d\sigma = \frac{d\sigma_{ii}}{3} \right) \tag{4.3}$$

where primes indicate deviatoric tensor components, S_{ijkl} is the compliance tensor, $\alpha_{ij}(\omega, \mathbf{x})$ is the thermal expansion coefficient (randomly specified in each grain), $\theta \ (= T - T_0)$ is the temperature change, f is the yield function, c is the yield limit, and G and K are the shear and bulk modulus, respectively. Here we assign randomness only in thermal expansion coefficients while keep other material parameters constant. This model also corresponds to a homogeneous media perturbed with random residual strains (thermal strain).

Regarding the loading of $\mathcal{B}$, we recall the Hill (-Mandel) condition [13,14], which guarantees the equivalence of energetically and mechanically defined effective responses

$$\overline{\boldsymbol{\sigma} : d\boldsymbol{\varepsilon}} = \int \overline{\boldsymbol{\sigma}} : d\overline{\boldsymbol{\varepsilon}} \Leftrightarrow \int_{\partial B_\delta} \left(\mathbf{t} - \overline{\boldsymbol{\sigma}} \cdot \mathbf{n} \right) \cdot \left(d\mathbf{u} - d\overline{\boldsymbol{\varepsilon}} \cdot \mathbf{x} \right) dS = 0 \tag{4.4}$$

where ∂B_δ is the boundary of a given specimen B_δ of size δ, $\mathbf{u}$ is the displacement vector, and $\mathbf{t}$ is the traction vector, both on the specimen boundary. This equation suggests three special types of uniform boundary conditions (BCs):

(i) uniform displacement BC:
$$d\mathbf{u} = d\bar{\boldsymbol{\varepsilon}} \cdot \mathbf{x} \qquad (4.5)$$

(ii) uniform traction BC:
$$\mathbf{t} = \bar{\boldsymbol{\sigma}} \cdot \mathbf{n} \qquad (4.6)$$

(iii) uniform mixed-orthogonal BC:
$$(\mathbf{t} - \bar{\boldsymbol{\sigma}} \cdot \mathbf{n}) \cdot (d\mathbf{u} - d\bar{\boldsymbol{\varepsilon}} \cdot \mathbf{x}) = 0 \qquad (4.7)$$

4.2 Numerical simulations

4.2.1 Observation of fractal patterns

A numerical study of the elastic-plastic transition, in plane strain, is carried out by ABAQUS [23]. The domain comprises 256×256 square-shaped grains, i.e., sufficiently large to compute fractal dimensions. Each individual grain is homogeneous and isotropic, its thermal expansion coefficient α being a uniform random variable from a range of up to $\pm 2.5\%$ about the mean and other material parameters being constant. The mean values are taken from 'ABAQUS Example Manual 5.1.2':

$$E = 93.5\,GPa, h = 76.5\,GPa, c = 153\,MPa, \alpha = 11.7 \times 10^{-6}\,/\,K, \upsilon = 0.27.$$

The temperature change is set to be $\theta = 20K$ up from $T_0 = 273.15K$. We apply shear loading through one of two types of uniform BCs consistent with Eqs. (4.5,4.6):

Displacement: $d\bar{\varepsilon}_{11} = -d\bar{\varepsilon}_{22} = d\varepsilon^0,\ d\bar{\varepsilon}_{12} = 0,$ (4.8)

Traction: $\bar{\sigma}_{11} = -\bar{\sigma}_{22} = \sigma^0,\ \bar{\sigma}_{12} = 0.$ (4.9)

Figures 4.1(a-d) show elastic-plastic transition patterns for increasing stress σ^0 under traction BC. The figures use a binary format in the sense that elastic grains are white, while the plastic ones are black. As the loading increases, the set of plastic grains grows with an apparently disordered geometry. Its fractal dimension D is estimated using a "box-counting method" [26].

Table 4.1 shows fractal dimensions and correlation coefficients for linear fits applied to each of Figs. 4.1(a-d) – the fractal character of sets of plastic grains is evident. The same type of results is obtained for displacement BC, whereby the spread of plastic grains is initially faster.

Figures 4.2(a,b) show response curves under these two BCs in terms of volume-averaged stress *vs.* strain and fractal dimension D *vs.* strain, respectively. The responses of single grain homogeneous phases are also given for a reference. We find that the responses of random heterogeneous materials all display smooth curves tending towards the line of homogeneous phases, which, in fact, is more realistic, since in real materials the elastic-plastic transition must develop smoothly rather than instantly. The constitutive response under displacement BC bound that under traction BC from above. This can be described by hierarchies of bounds for elastic-hardening plastic composites [20]. While the discrepancy is found to be larger here since for thermoelastic-plastic materials we need a larger size of RVE [12]. The fractal dimension D grows slower under the traction BC than the displacement BC, which corresponds to the characteristics of constitutive responses. However, note that they share a common trend regardless of the loading applied: D tends to 2.0 during the transition, showing that the plastic grains have a tendency to spread over the entire material domain. On the other hand, if we look at the evolution of elastic grains (the white set in Fig 4.1), it still shows to be a fractal with the dimension D decreasing from 2 to 0, see Fig. 4.3. We note that although the sets of elastic and plastic grains are complementary in the plane, the sum of their fractal dimensions does not necessarily give 2, indeed only at the beginning or in the end when no plastic regions or elastic domains exist.

4.2.2 Study of material randomness

Now we examine the elastic-plastic transition under different model configurations. First, the sensitivity to the material's model randomness is studied through a comparison of three cases: A1-α up to $\pm 2.5\%$ about the mean, $\theta = 20K$.

A2- α up to $\pm 12.5\%$ about the mean, $\theta = 20K$.

A3- Same variance of α to case 1, but $\theta = 100K$.

Note that, according to Eq.(4.2), the response is affected by the multiplicity $\alpha\theta$ as a whole. Cases A2 and A3 are thus assigned with same variance $\Delta(\alpha\theta)$ but for the latter the mean $\alpha\theta$ is higher. Results for A1-A3 are shown in Figs. 4.4(a, b). We find that different randomness in the model configuration lead to quantitatively, but not qualitatively different transition patterns. Basically, a lower randomness results in a narrower elastic-plastic transition, and the mean value of $\alpha\theta$ takes a stronger effect when the absolute variance is fixed – both, in curves of the average stress as well as the fractal dimension vs. the average strain.

Next, we study the transition patterns in different materials. This involves a comparison of the original material A1 with three other hypothetical materials:

B1- $E = 207 GPa, \alpha = 13.5e - 6/K$; $E/h, \alpha/(c/E)$ are the same with A1, i.e., $h = 169.36 GPa, \quad c = 390.84 MPa$.

B2- Same as B1 but with lower c : $c = 312.67 MPa$.

B3- Same as B1 but with lower h : $h = 135.49 GPa$.

Figures 4.5(a, b) show the resulting averaged stress-strain and fractal dimension vs. strain curves for these materials. We observe that the curves of material A1 and B1 are very close to each other and both bounded from below by those of materials B2 and B3. Thus, we conclude that higher E/h and/or $\alpha/(c/E)$ result in a slower elastic-plastic transition, a fact which is understandable, since under these circumstances the thermal fluctuation has a stronger effect in the elastic-plastic response. Also note that the homogeneous responses in stress-strain curves are distinct between materials B1 and B3 while in fractal dimension vs. strain responses they are the same. Based on these observations, we argue that the fractal dimension D can best be used to describe the transition patterns in a unified way for all the materials.

4.3 Summary

We consider elastic-plastic transitions in random, linear thermoelastic-hardening plastic media, where the thermal expansion coefficient (and/or elastic/plastic moduli, plastic limits) is taken as a strict-white-noise (non-fractal) random field. By setting up two types of monotonic loadings (either displacement or traction) consistent with the Hill-Mandel condition, we find that the set of plastic zones is a fractal with its dimension increasing towards 2.0. A gradual transition of the material from elastic type to plastic type, where plasticity spreads in a plane-filling fashion, is far more realistic than the idealized homogeneous medium model in which the transition is an immediate process, characterized by a kink in the stress-strain curve. For completeness we also study the complementary set (elastic regions) and observe that it is an evolving fractal with the dimension decreasing towards 0. Finally, with the fractal dimension parameter we further investigate elastic-plastic transitions by varying model randomness or material constants. It is observed that when the effect of random thermal fluctuations increases, as represented by a higher coefficient of variation of E/h and/or $\alpha/(c/E)$, the elastic-plastic transition process becomes slower.

Table 4.1: Results of estimating fractal dimensions

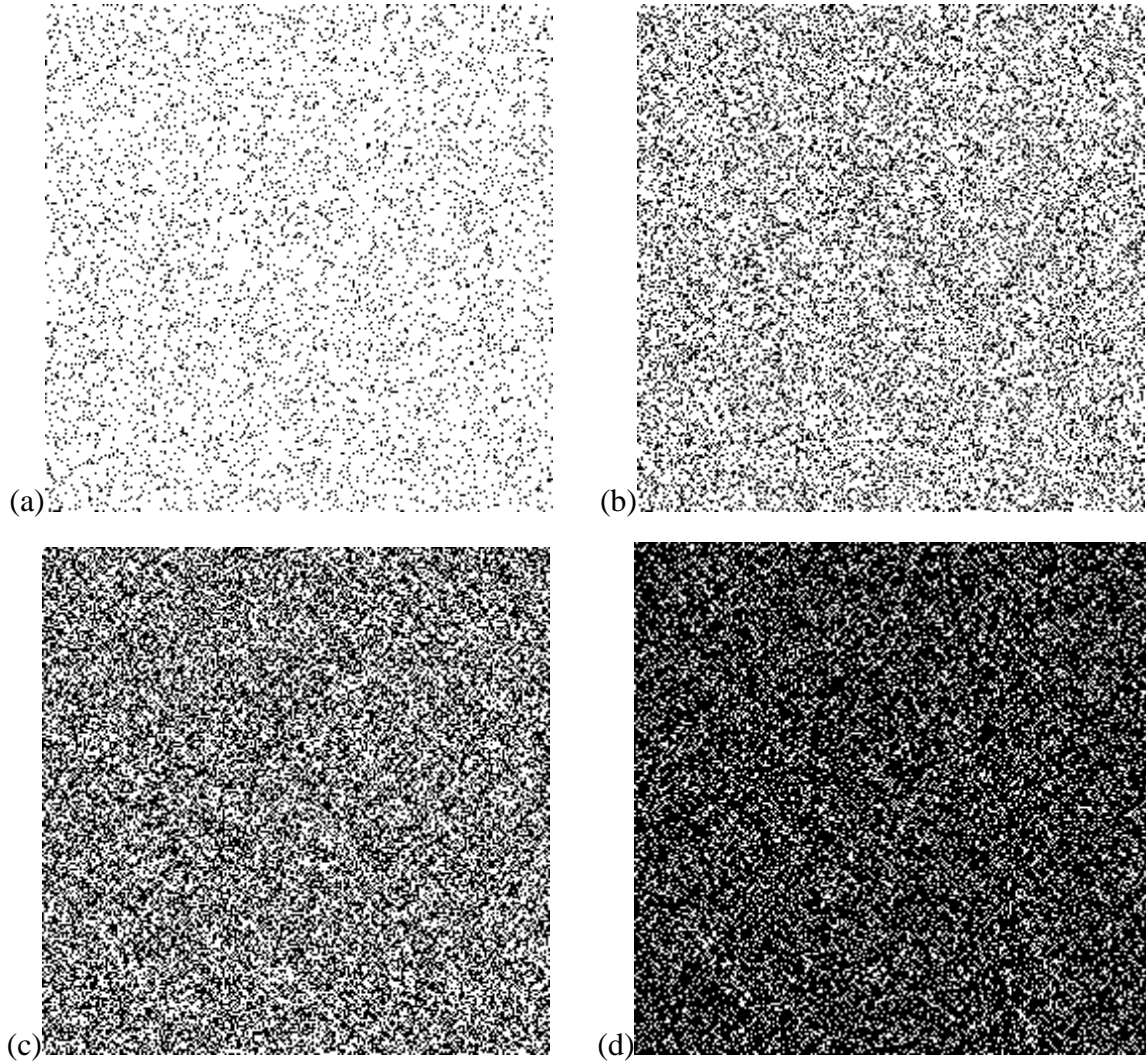|	Fig.4.1a	Fig.4.1b	Fig.4.1c	Fig.4.1d
Fractal dimension	1.8502	1.9477	1.9984	1.9999
Correlation coefficient	0.9970	0.9995	0.9999	1.0000

Figure 4.1: Field images (white/black: elastic/plastic) at the elastic-to-plastic transition under uniform traction BC at four consecutive levels of normalized average plastic strain $\overline{\varepsilon_p}$: (a) $\overline{\varepsilon_p} = 0.0001$, (b) $\overline{\varepsilon_p} = 0.0002$, (c) $\overline{\varepsilon_p} = 0.001$, (d) $\overline{\varepsilon_p} = 0.002$.
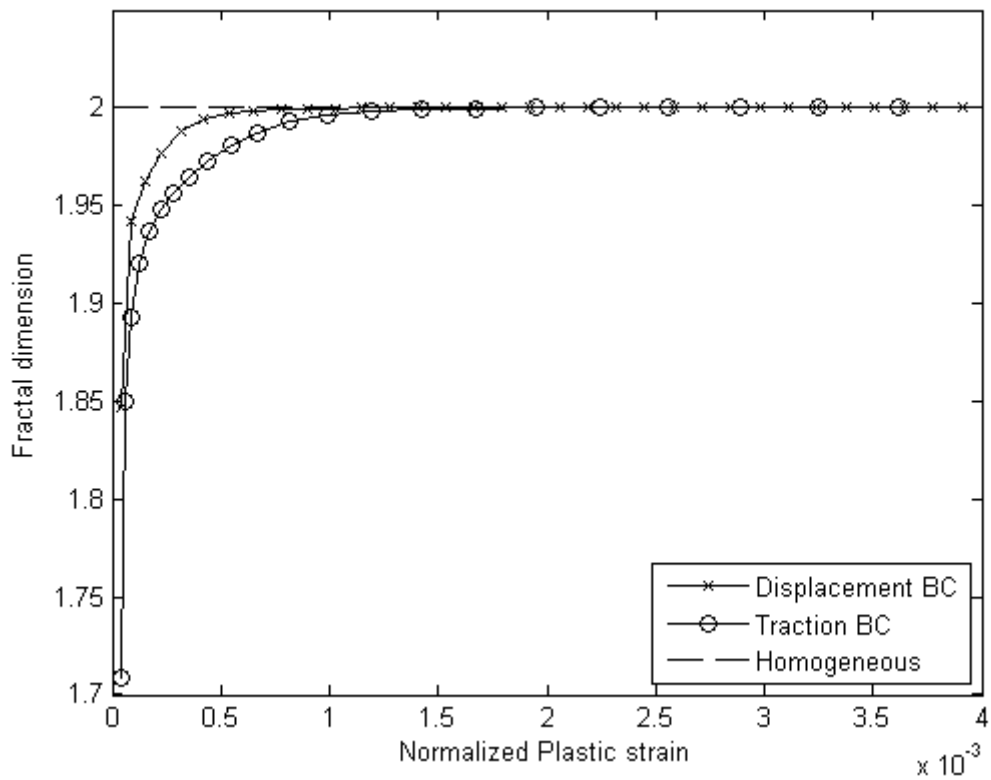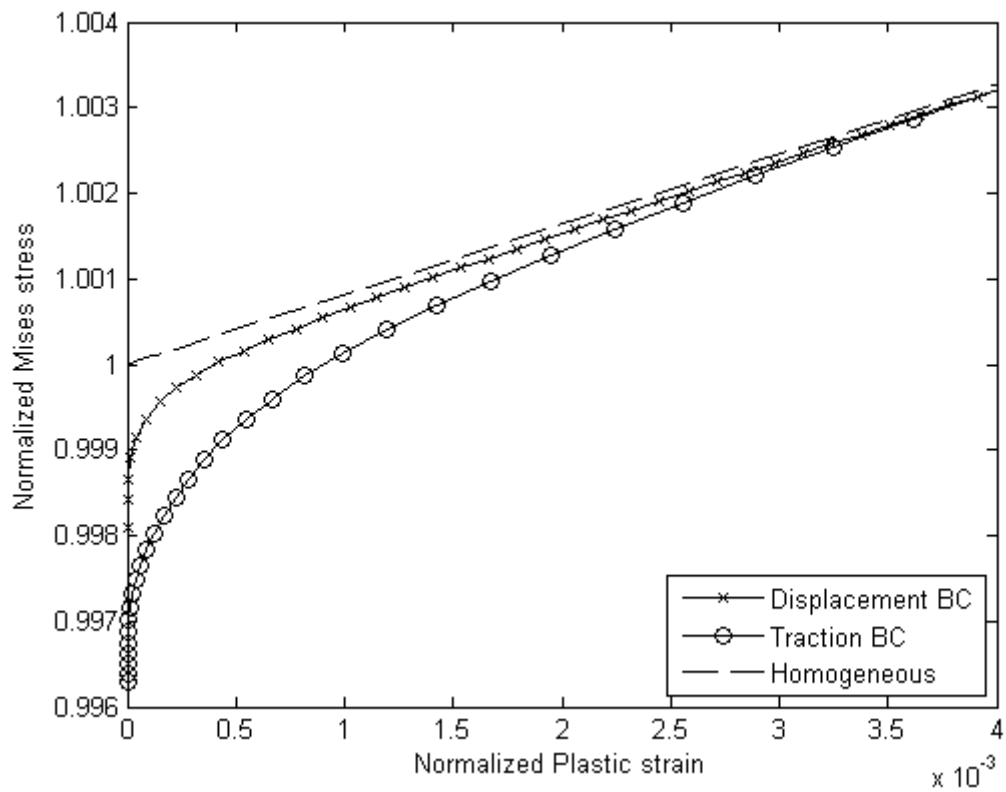
Figure 4.2: Response curves under different BCs: (a) Averaged stress~strain; (b)
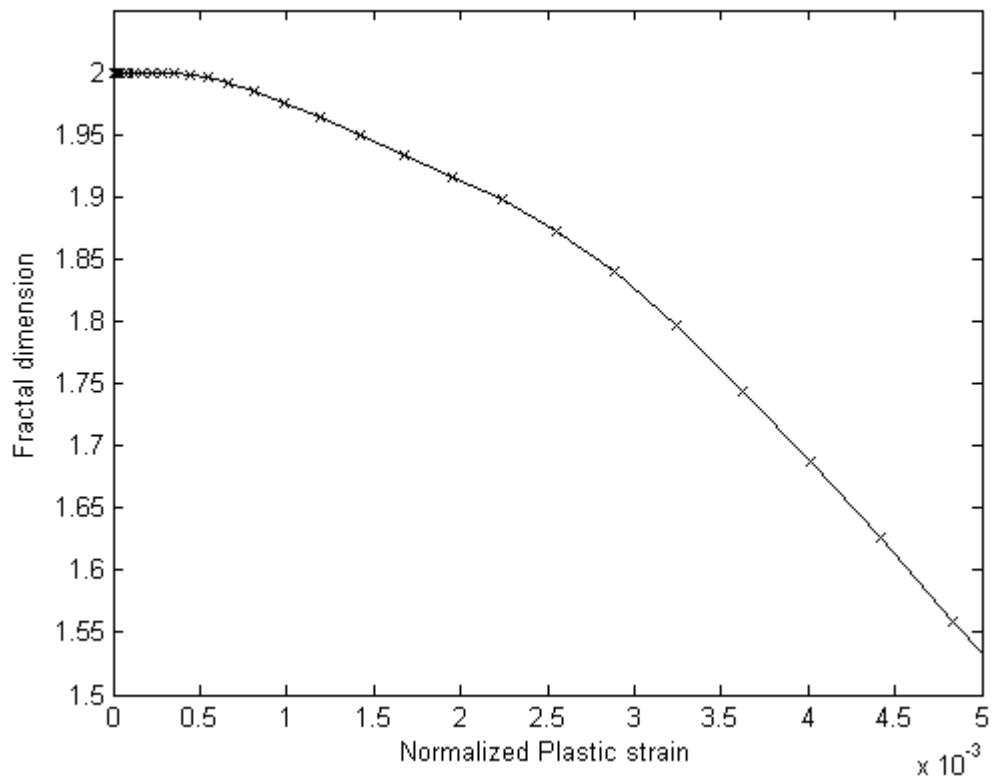
Fractal dimension~strain.

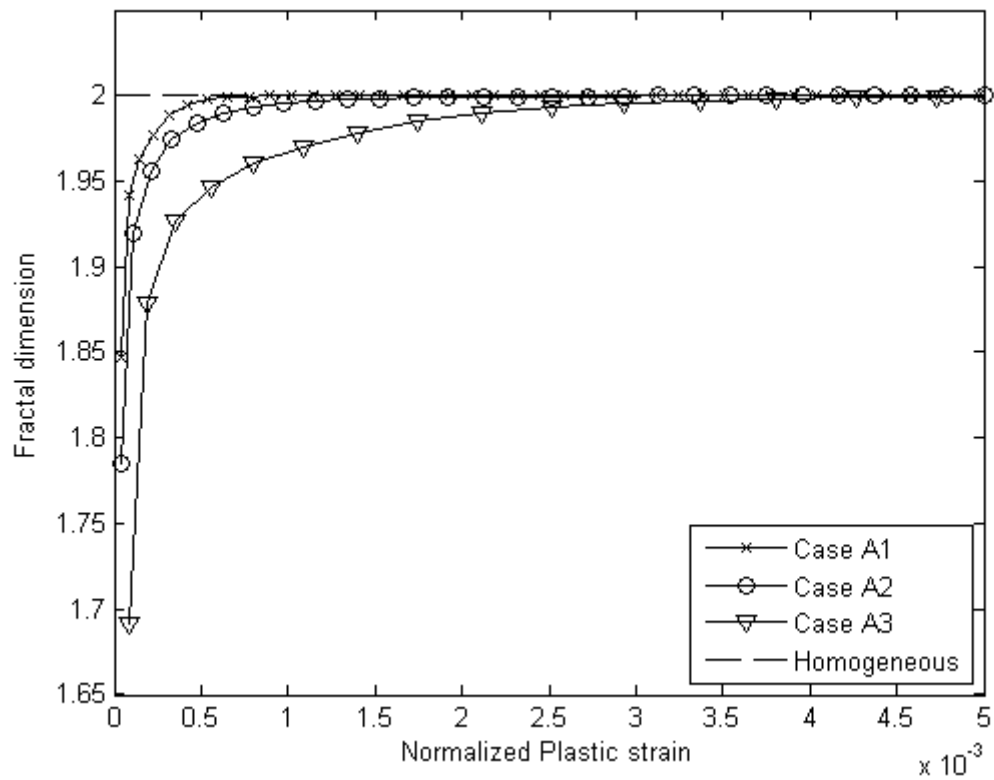Figure 4.3: Fractal dimension (elastic regions) versus normalized plastic strain curve.
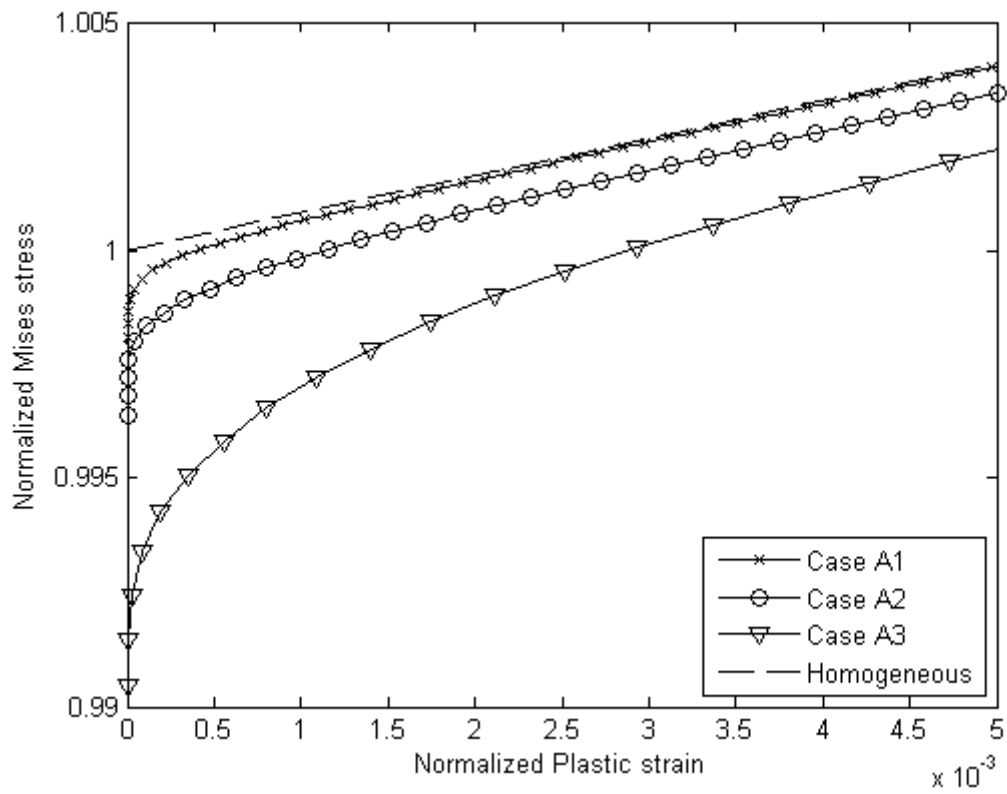
Figure 4.4: Comparison by different randomness: (a) Averaged stress~strain; (b) Fractal
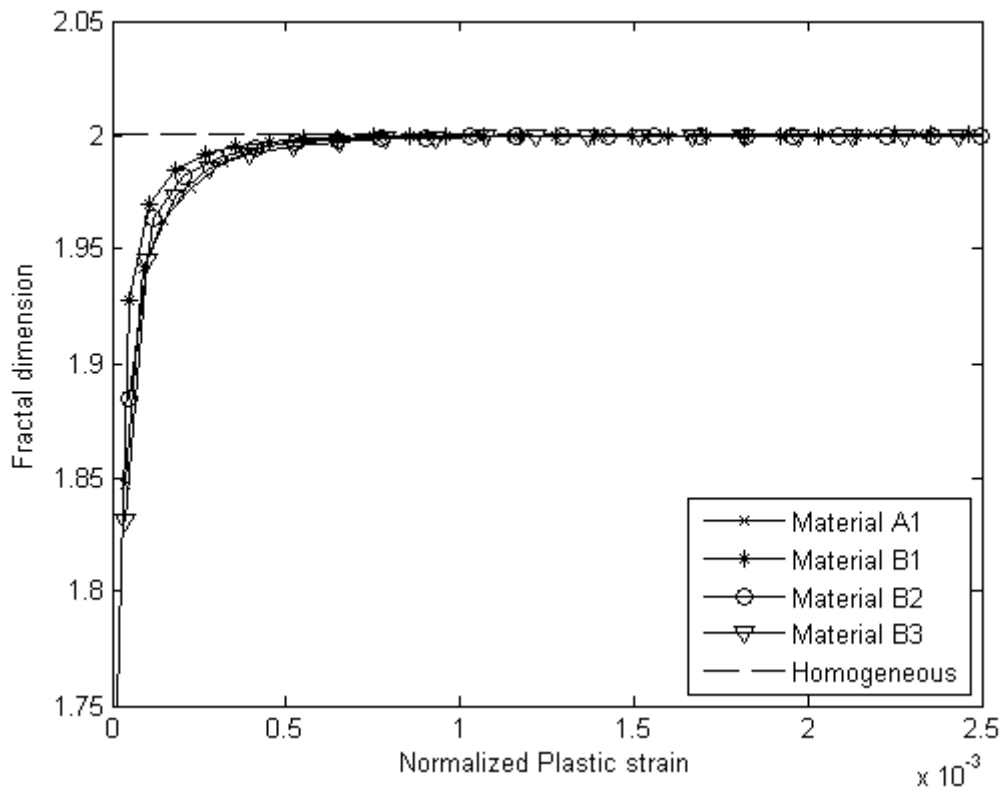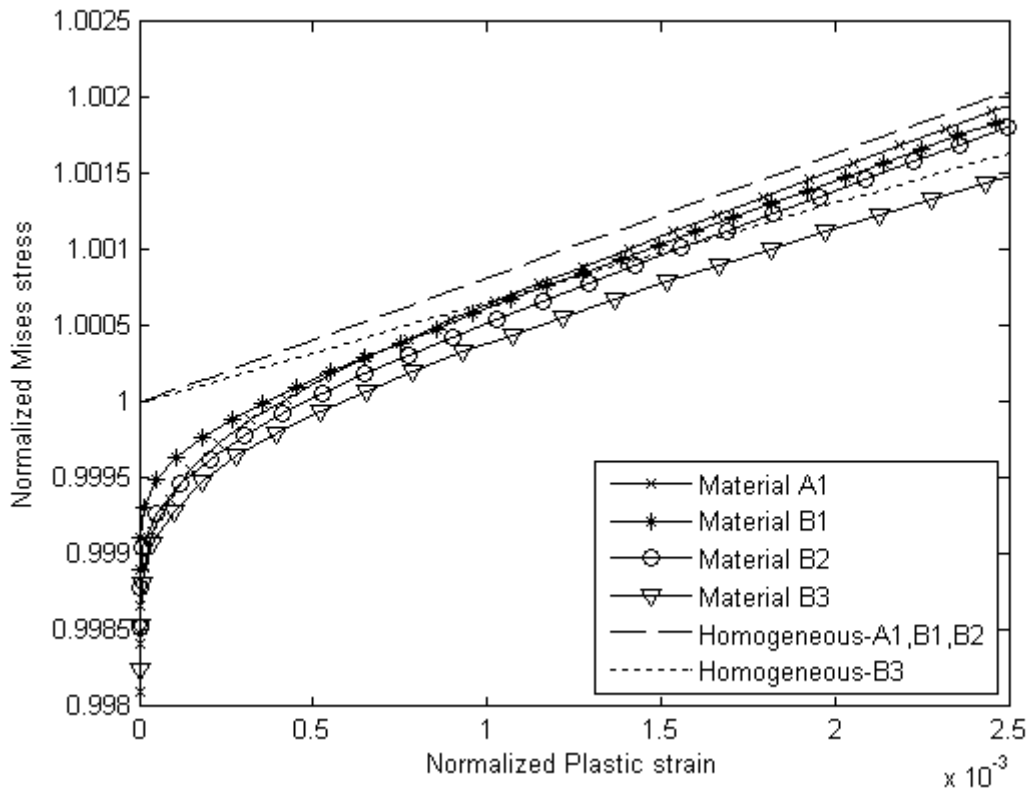
dimension~strain.

Figure 4.5: Comparison by different materials: (a) Averaged stress~strain; (b) Fractal dimension~strain.

CHAPTER 5

CONCLUSIONS

This thesis focuses on elastic-plastic transitions in random heterogeneous materials. In particular, we propose a fractal analysis methodology to investigate the transition pattern for a variety of random material models.

In Chapter 2, we first report on fractal patterns of plastic grains forming at elastic-plastic transitions in random elastic-perfectly plastic materials. Specifically, two models are considered – isotropic grains with weak random fluctuations in elastic moduli and/or yield limits and a polycrystal made of randomly oriented anisotropic grains. In both cases the lattice is subjected to pure shear loading increasing through either one of three macroscopically uniform boundary conditions (kinematic, mixed-orthogonal or static) admitted by the Hill-Mandel condition. Following the evolution of a set of plastic grains, we find that it is an evolving fractal with its fractal dimension increasing from 0 towards 2 as the material transitions from elastic to plastic. While the grains possess sharp elastic-plastic stress-strain curves, the overall responses are smooth and asymptote toward perfectly-plastic flows; these responses and the fractal dimension-strain curves are almost identical for three different loadings.

Chapter 3 continues the study of elastic-plastic transitions and proceeds to more realistic model materials with elastic-hardening plastic type. The focus is on isotropic grains in order to see the hardening effects clearly. By comparison study on models with different material configurations, we find that the hardening facilitates elastic-plastic

transitions – larger plastic modulus leads to a faster transition. The fractal analysis method demonstrates a very practical application: the curves of fractal dimension versus applied stress display a universal character for a range of different materials, thus providing a simple approach to infer the stress in materials at transitions. This chapter ends with a presentation of a Markov random field model of stochastic evolution of plastic grains to explain the fractal patterns.

In Chapter 4 we extend the investigation to thermo elastic-plastic media (or elastic-plastic materials with residual strains). A comparison study under various model randomness and material constants is conducted to demonstrate thermal elastic and hardening plastic effects altogether in elastic-plastic transitions. We show that the fractal dimension D can best be used to describe the transition patterns in a unified way for all different materials.

As mentioned in the Introduction of Chapter 1, the formation of fractal geometries was also studied in elastic-brittle materials in the eighties and nineties. It was found there that a fractal crack was approached only asymptotically, whereas at the elastic/plastic transitions the set of plastic grains is a continually evolving, and ultimately plane-filling fractal structure. That is, the fractal dimension of that set changes – indeed in elastic-perfectly plastic materials studied in Chapter 2, elastic-hardening-plastic type in Chapter 3, and thermo-elastic-plastic media (or elastic-plastic type with residual strains) shown in Chapter 5, as well as in several variations thereof. Considering that the magnitude of plastic strain is reflected in the strength of slip-lines and shear bands, we think that even very weak material randomness in material parameters of elastic-ductile materials causes plastic

slip-lines and shear bands to evolve as fractals.

At this point we can only conjecture that the plane-filling character becomes space-filling in three-dimensional settings, with simulations of the latter appearing to be barely within the reach of present day computers. Our current study is set in the context of metal materials, future studies will be conducted to incorporate crystal plasticity and soil mechanics models.

REFERENCES

[1]   Mandelbrot, B., 1982. *The Fractal Geometry of Nature*, W.H. Freeman & Co.

[2]   Feder, J., 2007. *Fractals (Physics of Solids and Liquids)*, Springer, New York.

[3]   Sornette, D. 2004. *Critical Phenomena in Natural Sciences*, Springer, New York.

[4]   Sahimi, M. and Goddard, J.D. 1986. Elastic percolation models for cohesive mechanical failure in heterogeneous systems, *Phys. Rev. B* **33**, 7848-7851.

[5]   Sahimi. M. 2003. *Heterogeneous Materials II*. Springer, New York.

[6]   Saouma, V.E. and Barton, C.C., 1994. Fractals, fractures, and size effects in concrete, *J. Eng. Mech. ASCE* **120**, 835-855.

[7]   Shaniavski, A.A. and Artamonov, M.A., 2004. Fractal dimensions for fatigue fracture surfaces performed on micro- and meso-scale levels, *Int. J. Fracture* **128**, 309-314.

[8]   Zaiser, M. Bay, K. & Hahner, P., 1999. Fractal analysis of deformation-induced dislocation patterns, *Acta. Mater.* **47**, 2463-2476.

[9]   Ostoja-Starzewski, M., 1990. Micromechanics model of ice fields - II: Monte Carlo simulation, *Pure Appl. Geophys.* **133**:2, 229-249.

[10]   Poliakov, A.N.B., Herrmann, H.J., Podladchikov, Y.Y. & Roux, S., 1994. Fractal plastic shear bands, *Fractals* **2**, 567-581.

[11]   Poliakov, A.N.B. & Herrmann, H.J., 1994. Self-organized criticality of plastic shear bands in rocks, *Geophys. Res. Lett.* **21**(19), 2143-2146.

[12]   Li, J. and Ostoja-Starzewski, M., 2010. Fractal pattern formation at elastic-plastic transition in heterogeneous materials, *ASME J. Appl. Mech.* **77**, 021005-1-7.

[13]   Hill, R., 1963. Elastic properties of reinforced solids: some theoretical principles, *J. Mech. Phys. Solids* **11**, 357-372.

[14]   Hazanov, S., 1998. Hill condition and overall properties of composites, *Arch. Appl. Mech.* **68**, 385-394.

[15]   Ostoja-Starzewski, M., 2008. *Microstructural Randomness and Scaling in Mechanics of Materials*, Chapman & Hall/CRC Press.

[16]   Podio-Guidugli, P., 2000. A primer in elasticity, *J. Elast.* **58**, 1-104.

[17] Huet, C., 1990. Application of variational concepts to size effects in elastic heterogeneous bodies. *J. Mech. Phys. Solids* **38,** 813-841.

[18] Ostoja-Starzewski, M. and Castro, J. 2003. Random formation, inelastic response and scale effects in paper, *Phil. Trans. R. Soc. A* **361**(1806), 965-986.

[19] Hazanov, S. & Huet, C., 1994, Order relationships for boundary conditions effect in heterogeneous bodies smaller than the representative volume. *J. Mech. Phys. Solids* **42**, 1995-2011.

[20] Jiang, M., Ostoja-Starzewski, M. & Jasiuk, I., 2001. Scale-dependent bounds on effective elastoplastic response of random composites, *J. Mech. Phys. Solids* **49**, 655-673.

[21] Taylor, L., Cao, J., Karafillis, A.P. & Boyce, M.C., 1995. Numerical simulations of sheet-metal forming, *J. Mater. Process. Tech.* **50**, 168-179.

[22] Shoemake, K., 1992. Uniform random rotations, in: D. Kirk (Ed.), *Graphics Gems* **III.** Academic Press.

[23] ABAQUS, 2008. ABAQUS User's Manual Version 6.8. Dassault Systèmes Simulia Corp., Providence, RI, USA.

[24] Jeulin, D. Li, W. & Ostoja-Starzewski, M., 2008. On the geodesic property of strain field patterns in elasto-plastic composites, *Proc. R. Soc. A* **464**, 1217-1227.

[25] Ostoja-Starzewski, M., 2005. Scale effects in plasticity of random media: Status and challenges, *Intl. J. Plast.* **21,** 1119-1160.

[26] Perrier, E., Tarquis, A.M. & Dathe, A., 2006. A program for fractal and multi-fractal analysis of two-dimensional binary images: Computer algorithms versus mathematical theory, *Geoderma* **134**, 284-294.

[27] Hill, R., 1951. The elastic behavior of a crystalline aggregate, *Proc. Phys. Soc.* A **65**, 349-354.

[28] Li, J. and Ostoja-Starzewski, M., 2009. Fractals in elastic-hardening plastic materials, *Proc. R. Soc. A*, in press.

[29] Simo, J.C. & Hughes, T.J.R., 1998. *Computational Inelasticity,* Springer, New York.

[30] Preston, C.J., 1974. *Gibbs states on countable sets*. Cambridge, UK: Cambridge University Press.

[31] Hammersley, J.M. and Mazzarino, G., 1983. Markov fields, correlated percolation, and the Ising model. In *The mathematics and physics of disordered media* (eds B. D. Hughes and B. W. Ninham). Lecture Notes in Mathematics, no. 1035, pp. 201–245. New York, NY: Springer-Verlag.

[32] Onural, L., 1991. Generating connected textured fractal patterns using Markov random fields. *IEEE*

Trans. Pattern Anal. Mach. Intell. **13**, 819–825.

[33] Ghozi, R., 2001. Fractal characterization of non-Gaussian critical Markov random fields. In *Int. Symp. on Signal Processing and its Applications*, vol. 2, pp. 663–666.

[34] Li J. and Ostoja-Starzewski, M., 2009. Fractal pattern formation in thermoelastic-plastic, heterogeneous materials. *Proceedings of the 8th International Congress on Thermal Stresses,* 283-286.